Monthly Notices of the ROYAL ASTRONOMICAL SOCIETY

MNRAS **553,** 1–15 (2026)
Advance Access publication 2026 October 23

https://doi.org/10.1093/mnras/stag2017

The ALMA REBELS survey: the [C II] luminosity function of UV-selected galaxies at $z \sim 7$

Thomas Herard-Demanche [1]★ Pascal A. Oesch [2,3] Rychard Bouwens,[1] Jacqueline A. Hodge,[1] Hiddo S. B. Algera [4] Manuel Aravena,[5,6] Karin Cescon [1] Elisabete da Cunha [7,8] Pratika Dayal [9,10,11] Andrea Ferrara,[12] Rebecca Fisher [13] Yoshinobu Fudamoto,[14] Kasper E. Heintz [3] Hanae Inami [15] Andrea Pallottini [16] Lucie E. Rowland [1] Renske Smit,[17] Laura Sommovigo [18,19] Mauro Stefanon,[20,21] Michael W. Topping [22] Paul van der Werf[1] and Ivana F. van Leeuwen [1]

Affiliations are listed at the end of the paper

Accepted 2026 October 14. Received 2026 October 3; in original form 2026 July 15

ABSTRACT

Luminosity functions (LF) are some of the most basic quantities providing insights into galaxy evolution across cosmic time and enabling a direct comparison between observations and simulations. Here, we present the first [C II] 158 μm LF at $z \sim 7$ from a sizeable ultraviolet (UV)-selected Atacama Large Millimeter/submillimeter Array (ALMA) sample. Our analysis makes use of 27 galaxies with significant [C II] emission line detections in the epoch of reionization from the Reionization Era Bright Emission Line Survey (REBELS) ALMA Large Programme and its pilot programmes. We used these line detections and other [C II] detections from the literature to calibrate UV luminosity-$L_{[\mathrm{C\,II}]}$ and stellar mass-$L_{[\mathrm{C\,II}]}$ relations at $z \sim 7$. Given the challenge in precisely defining a selection volume for the REBELS sample itself, we rely on published UV LF and stellar mass function (SMF) determinations at $z \sim 7$ and three complementary approaches to derive the [C II] LF. The UV-LF-based method provides a lower limit on the [C II] LF, due to its missing the most dust-obscured systems. Our SMF-based estimate yields a Schechter function with a characteristic luminosity of $L^*_{[\mathrm{C\,II}]} = 10^{9.11^{+0.11}_{-0.27}}\,\mathrm{L}_\odot$ and a steep faint-end slope. From $z \sim 7$ to $z \sim 5$, our inferred [C II] LF shows an evolution of +0.3 dex in normalization and +0.1 dex in $L^*_{[\mathrm{C\,II}]}$. Our results indicate a general underprediction from models of the abundance of [C II] emitters at high-redshift and thus potentially the number densities of massive yet UV-faint systems implied by our SMF-based method. Additionally, they suggest that 63 per cent of the star formation rate density occurs in massive [C II]-bright systems and that ∼60per cent to 90 per cent of [C II] emitters at $z \sim 7$ may be missed by bright UV selections. This highlights the importance of surveys focusing on especially massive, UV-faint sources at $z > 6$.

Key words: galaxies: abundances – galaxies: evolution – galaxies: high-redshift – galaxies: ISM – galaxies: star formation.

1 INTRODUCTION

The detailed characterization of the first generation of galaxies is one of the prime goals of observational astrophysics. Great progress has been achieved to reveal the star-formation rates (SFR) and stellar masses of galaxies in the epoch of reionization (EoR) based on large galaxy samples selected from the *Hubble Space Telescope* (*HST*) and the *James Webb Space Telescope* (*JWST*) out to the highest redshifts (e.g. P. Dayal & A. Ferrara 2018; B. E. Robertson 2022; J. Matthee 2025; D. P. Stark et al. 2026). However, the interstellar medium (ISM) properties of these early sources are more difficult to study (e.g. C. L. Carilli & F. Walter 2013; J. A. Hodge & E. da Cunha 2020).

Evidence has emerged that the ISM conditions of $z > 6$ galaxies differed significantly compared to their descendants at later cosmic epochs. These systems exhibit intense nebular emission, high ionization parameters, hard radiation fields produced by young massive stars, elevated electron densities and rapid chemical enrichment despite their young ages (e.g. A. J. Cameron et al. 2023; M. Curti et al. 2023; K. E. Heintz et al. 2024; R. L. Sanders et al. 2024; A. L. Faisst et al. 2026; L. E. Rowland et al. 2026; T. M. Stanton et al. 2026). Together, these observations point to compact, gas-rich galaxies with highly dynamic interstellar media that likely promoted efficient star formation and strong stellar feedback during the first few hundred million years of cosmic history.

The revolutionary sensitivity of ALMA is now providing detailed insights into the chemical and physical properties of early galaxies, in particular, with the use of the [C II] emission line at 158 μm.

★ E-mail: herard@strw.leidenuniv.nl

© The Author(s) 2026.
Published by Oxford University Press on behalf of Royal Astronomical Society. This is an Open Access article distributed under the terms of the Creative Commons Attribution License (https://creativecommons.org/licenses/by/4.0/), which permits unrestricted reuse, distribution, and reproduction in any medium, provided the original work is properly cited.

Downloaded from academic.oup.com/mnras/article/553/2/stag2017/8994297 by Liverpool John Moores University user on 16 November 2026

[C II] is the dominant cooling line of the ISM, coming primarily from photodissociation regions and the cold neutral medium of molecular clouds (e.g. M. G. Wolfire et al. 1995; D. J. Hollenbach & A. G. G. M. Tielens 1999; M. G. Wolfire, L. Vallini & M. Chevance 2022). However, the relative contributions from different ISM phases to the [C II] emission could well differ at higher redshifts compared to the local Universe (e.g. L. Vallini et al. 2018; A. Ferrara et al. 2019; H. Katz et al. 2019; A. Pallottini et al. 2022; A. F. Ramos Padilla et al. 2023). Nevertheless, [C II] correlates surprisingly well with the star formation rates of galaxies out to the highest redshifts (see e.g. G. J. Stacey et al. 1991; I. De Looze et al. 2014; P. L. Capak et al. 2015; R. Herrera-Camus et al. 2015; S. Carniani et al. 2018; J. Matthee et al. 2019; D. Schaerer et al. 2020; M. Romano et al. 2022). Beyond SFR, [C II] has been used to estimate molecular gas masses (e.g. A. Zanella et al. 2018; M. Dessauges-Zavadsky et al. 2020; L. Vallini et al. 2025), outflows (e.g. S. Gallerani et al. 2018; M. Ginolfi et al. 2020; E. Pizzati et al. 2023), the extended ISM (e.g. S. Fujimoto et al. 2019; Y. Fudamoto et al. 2022), and even neutral gas and metal content (K. E. Heintz et al. 2021, 2023; L. Vallini et al. 2024).

Dedicated ALMA programmes have applied these diagnostics to the earliest massive, star-forming galaxies. The Reionization Era Bright Emission Line Survey (REBELS; R. J. Bouwens et al. 2022a), in particular, has revealed that ultraviolet (UV)-luminous $z \sim 7$ galaxies host large molecular gas reservoirs ($M_{\rm mol} \sim 10^{10.5}$-$10^{11}$ $M_\odot$; M. Aravena et al. 2024; K. Cescon et al. 2026), together with significant dust masses and elevated dust temperatures ($T_{\rm d} \sim 40$–60 K; H. Inami et al. 2022; L. Sommovigo et al. 2022). Between 30 per cent and 90 per cent of their star formation is dust-obscured, depending on stellar mass (H. S. B. Algera et al. 2023; R. A. A. Bowler et al. 2024). High-resolution follow-up of the most [C II]-luminous source, REBELS-25 at $z = 7.31$, has further uncovered a fully assembled, dynamically cold rotating disc with $V_{\rm rot}/\sigma \approx 11$ (L. E. Rowland et al. 2024). Taken together, these results show that massive, gas-rich, dusty and kinematically mature systems are already in place within the first billion years of cosmic time.

JWST is now providing a complementary, rest-frame optical view of these same systems. Through the REBELS-IFU programme, NIRSpec integral field unit (IFU) spectroscopy has delivered gas-phase metallicities, demonstrating that an enriched mass–metallicity relation is already in place at $z \sim 7$ (L. E. Rowland et al. 2026), the first direct constraints on their dust attenuation curves (V. Markov et al. 2023, 2025; R. Fisher et al. 2025; I. Shivaei et al. 2026), and scaling relations between dust, gas, and metals that begin to disentangle the dominant dust-production pathways at these epochs (H. S. B. Algera et al. 2026). Together, ALMA and *JWST* are therefore enabling a panchromatic characterization of the most massive star-forming galaxies in the EoR.

Alongside these UV-selected [C II] emitters, however, ALMA and *JWST* have also revealed populations of heavily dust-obscured galaxies that evade UV-selection altogether (L. Barrufet et al. 2023a; T. Herard-Demanche et al. 2025). These, along with serendipitously identified companions to targeted [C II] systems may contribute a non-negligible fraction of the integrated stellar mass (R. Gottumukkala et al. 2024), star formation rate density (SFRD; I. F. van Leeuwen et al. 2024), and must be accounted for in any complete census of star-forming systems in the EoR.

The [C II] line offers several advantages for such a census: It is unaffected by dust attenuation, and falls in a favourable ALMA frequency window, when redshifted to $z = 6$-8 in the heart of the EoR. It has thus been widely used both to probe the ISM of early galaxies and to secure their redshifts (e.g. R. Maiolino et al. 2015; S. Carniani et al. 2018; T. Hashimoto et al. 2019; T. J. L. C. Bakx et al. 2020; O. Le Fèvre et al. 2020; R. J. Bouwens et al. 2022a; R. Herrera-Camus et al. 2025). First [C II] luminosity functions (LF) have been measured up to $z \sim 6$ from the ALMA Large Program to INvestigate [C II] at Early times (ALPINE) survey (L. Yan et al. 2020), while at $z = 6$-8 only upper limits exist so far (e.g. Y. Yamaguchi et al. 2017; B. D. Uzgil et al. 2021). Measurements at these epochs offer particularly powerful constraints on theoretical models and cosmological simulations, which at present predict widely differing LFs at these redshifts, as we show in the later sections.

In this paper, we exploit the ALMA–*JWST* synergy outlined above to derive the first [C II] LF at $z \sim 7$, leveraging data from the REBELS ALMA Cycle-7 Large Programme and its pilot programmes. To account both for the UV-luminous massive galaxies that dominate REBELS and for the dust-obscured population largely missed by UV-selected surveys, we complement the sample with a *JWST*-derived galaxy stellar mass function (SMF; A. Weibel et al. 2024). We apply multiple complementary methods, including the approach developed by L. Yan et al. (2020) for the ALPINE sample at $z \sim 4$-6 (M. Béthermin et al. 2020; A. L. Faisst et al. 2020; O. Le Fèvre et al. 2020), to derive LFs in our measurement range using the UV LF at this epoch as proxy and help constrain the intrinsic [C II] LF in the EoR. This paper is organized as follows: In Section 2, we describe the galaxy sample. In Section 3, we describe our approach to derive the [C II] LF, before we compare our results with other works in Section 4 and conclude in Section 5. Throughout this paper, magnitudes are given in the AB system and the adopted cosmological parameters are $\Omega_{\Lambda,0} = 0.7$, $\Omega_{\rm M,0} = 0.3$, $H_0 = 70\,{\rm km\,s^{-1}\,Mpc^{-1}}$.

2 OBSERVATIONAL DATA

2.1 REBELS $z \sim 7$ sample

The primary data set for this paper is based on the ALMA Large programme REBELS (R. J. Bouwens et al. 2022a), as well as its pilot programmes (R. Smit et al. 2018; S. Schouws et al. 2022, 2023). These programmes selected a sample of 40 (REBELS) and nine (pilot) UV luminous galaxies with photometric redshifts $z > 6.5$ for ALMA line scan follow-up. In total $\sim$7 deg^2 of ground-based imaging was used to identify the best targets, with accurate photometric redshift estimates. The presence of strong rest-frame optical line emission and a sharp Lyman-break were both of significant utility in ensuring the accuracy of our photometric redshift estimates. The total REBELS sample spans a range of UV absolute magnitudes $M_{\rm UV} = -23.0$ to -21.3 and redshifts $z = 6.4$-8.6. Their stellar masses and star-formation rates place them at the high end of the main sequence of star formation at these redshifts (M. W. Topping et al. 2021; R. J. Bouwens et al. 2022a).

For sources in the redshift range $z = 6.4$-7.7, a scan is conducted for the [C II] 158 μm emission line in frequency windows spanning the photometric redshift probability distribution function of the target galaxies. For higher redshift sources ($z > 7.7$), the spectral scans focused on the [O III] 88 μm line (I. F. van Leeuwen et al. 2025). Given the differences in emission line strengths and sky transparency at the specific observed wavelengths, this is the most efficient approach for detecting ISM cooling lines for galaxies at $z > 6$, while also probing the dust continua. The typical [C II] luminosity limits of the REBELS line

Downloaded from academic.oup.com/mnras/article/553/2/stag2017/8994297 by Liverpool John Moores University user on 16 November 2026

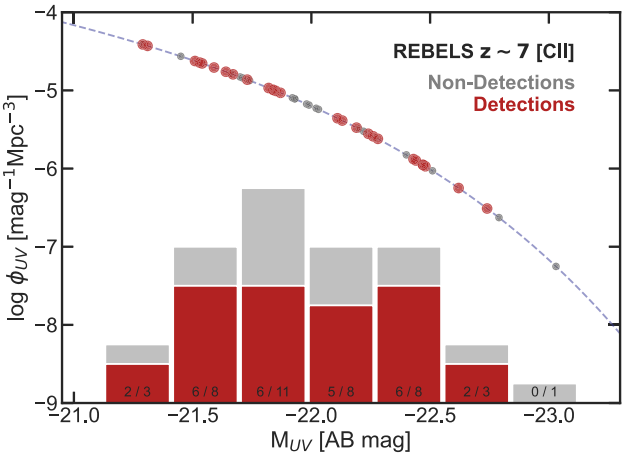


Figure 1. Histogram of the REBELS + pilot [C II] detected versus non-detected galaxies as a function of the absolute magnitude $M_{\rm UV}$ in the rest-UV. The red-shaded area shows the detections (>4σ), while grey corresponds to non-detections. The numbers presented at the base of the histogram indicate the number of [C II]-detected galaxies relative to total numbers in each $M_{\rm UV}$ bin. Generally, the detection fraction seems to be independent of UV luminosity. The dashed line further shows the UV luminosity function from R. J. Bouwens et al. (2021). The small red and grey dots indicate the locations of REBELS targets for detected and non-detected galaxies, respectively. Our method of estimating a step-wise [C II] LF is based on the expected numbers of galaxies in $M_{\rm UV}$ bins based on the UV LF (see Section 3.3 for more details).

scans are $\sim 3 \times 10^8$ L$_\odot$. R. J. Bouwens et al. (2022a) present the spectral windows used for the line scans relative to the photometric redshift probability distribution functions. Meanwhile, the dust continuum detections are described in H. Inami et al. (2022). In addition to the [C II] luminosities of the REBELS galaxies, we also make use of their stellar masses and absolute UV magnitudes derived from spectral energy distribution (SED) fitting from M. W. Topping et al. (2022). These fits are primarily based on ground-based photometry supplemented by Spitzer/IRAC and *HST*/ACS and WFC3 data where available (M. W. Topping et al. 2022; R. J. Bouwens et al. 2022a). The fits are performed at the [C II] redshift for the sources considered in this work.

2.2 [C II] emission line sample

In this paper, we only focus on the galaxy sample for which we have searched for [C II] emission lines, i.e. with either photometric or spectroscopic redshifts $z = 6.4$-7.7. This includes 42 sources in total, 35 and 7 of which are from the REBELS and pilot programmes, respectively. We refer the reader to S. Schouws et al. (in preparation) for details of the [C II] emission line measurements. The line sensitivity limit can vary significantly from source to source, with a median 4σ line sensitivity of 280 mJy km s^{-1}, corresponding to a luminosity limit of $\log(L_{\rm [C\,II]}/{\rm L}_\odot) = 8.6$.

The spectroscopic success rate for a significant detection of a [C II] line at >4σ is 64 per cent with little indication that this success rate depends on UV luminosity (see Fig. 1). Therefore, a total of 27 sources have obtained new spectroscopic redshift measurements thanks to REBELS and its pilots (22 and 5, respectively; see S. Schouws et al., in preparation). These 27 [C II] detected galaxies provide the main sample for this work. The mean redshift of these sources is $z_{\rm [C\,II]} = 6.94$ and span the redshift range $z = 6.50$-7.68. Note that we do not use the remaining REBELS sources that did not reveal a detectable [C II] line, since we cannot be sure whether the line was not detected due to its faintness or because we have not scanned at the proper redshifted frequency given the photometric redshift probability distribution function. There is some evidence that the former applies in many cases: The lack of continuum detections among the [C II]-undetected sources suggests that most may genuinely fall below the [C II] detection limit, in which case their exclusion would systematically bias $L_{\rm [C\,II]}/L_{\rm UV}$ high. Unfortunately, this cannot presently be established with certainty for individual non-detections, while treating all of them as intrinsically [C II]-faint would introduce a bias in the opposite direction.

2.3 $z \sim$ 4–6 galaxies from ALPINE

In addition to the REBELS $z \sim 7$ galaxy sample, we also consider the publicly available catalogues from the ALPINE large programme[1] for lower redshift comparisons (O. Le Fèvre et al. 2020). In particular, ALPINE targeted the [C II] emission line of 118 galaxies on the main sequence with pre-existing spectroscopic redshifts in the range $z_{\rm spec} = 4.4$-5.9 (see M. Béthermin et al. 2020; A. L. Faisst et al. 2020 for the [C II] catalogues and ancillary data analysis, respectively). In the following, we make use of the UV magnitudes and stellar masses of the ALPINE galaxies derived from the LePhare SED fits (A. L. Faisst et al. 2020). The UV magnitude range of ALPINE includes somewhat fainter ($M_{\rm UV} \sim -20.5$ mag) sources than REBELS does. Nevertheless, the overall success rate of ALPINE for [C II] detections is almost exactly the same (64 per cent) as for the REBELS sample at $z \sim 7$, resulting in 75 [C II] (>3σ) detections and 43 non-detections, for which conservative upper limits on [C II] are derived (see M. Béthermin et al. 2020, for details).

A comparison of the ALPINE and REBELS targets can be seen in Fig. 2. At fixed UV luminosity, the two samples show consistent [C II] luminosities, which span a very similar range. However, the ALPINE sample extends to lower UV luminosities, while for the REBELS sample bright [C II] emitters make up a higher percentage of the total sample. Despite this, the two samples span a similar range in stellar mass. We will thus use these measurements to derive a relation between both the UV and [C II] luminosities and the $M_\star$ and [C II] luminosities (see Sections 3.1 and 3.2).

3 ESTIMATES OF THE [C II] LUMINOSITY FUNCTION

In this section, we describe three methods to determine the [C II] LF at $z \sim 7$ based on the REBELS results. The main challenge with this endeavour is that the REBELS targets were identified from rest-UV observations over a 7 deg^2 area and no equivalent survey for the [C II] line exists over the same volume. One way of circumventing these challenges is by tying the derivation of the [C II] LF to galaxy distribution functions. The latter functions will be used to provide a representative volume for each source. Our first two approaches, both based on empirical modelling, are identical in structure but use different ingredients. In those two empirical modellings, we convert a galaxy distribution function based on a certain galaxy property, i.e. UV luminosity or stellar mass, into a [C II] LF with the use of an empirical relation on

[1] https://cesam.lam.fr/a2c2s/data_release.php

Downloaded from academic.oup.com/mnras/article/553/2/stag2017/8994297 by Liverpool John Moores University user on 16 November 2026

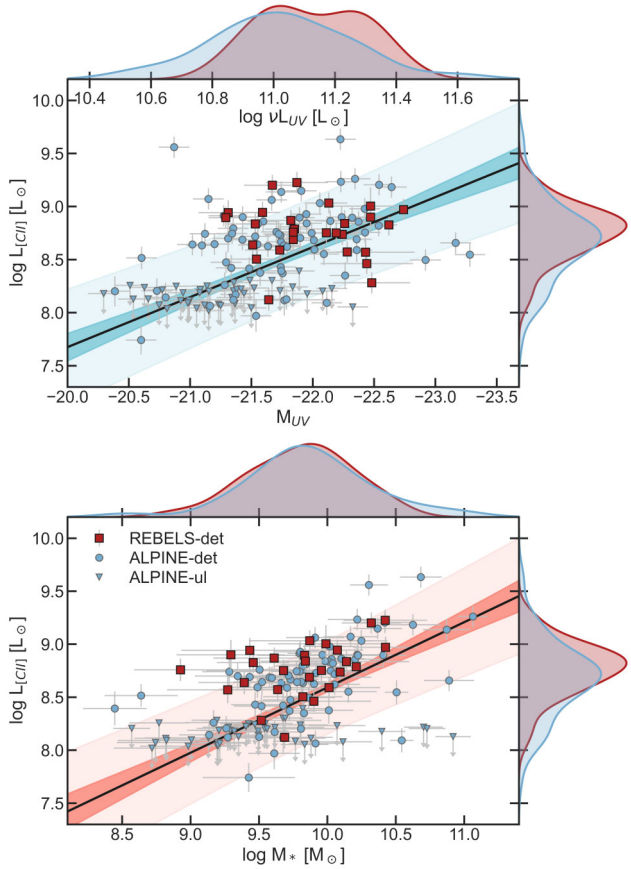


Figure 2. Empirical relations between rest-frame UV and [C II] luminosity (upper), and stellar mass and [C II] luminosity (lower) for sources at $z = 4$-8 based on the ALPINE and REBELS galaxy samples. The smoothed distribution using kernel density estimation for $L_{[\mathrm{C\,II}]}$, $M_\star$, and M_{UV} is shown on the right side and the top of each figure. Blue points and triangles correspond to the ALPINE $z = 4$-6 [C II] detections and 3σ upper limits, respectively. The red squares are the REBELS $z \sim 7$ galaxies with [C II] detections. The modelled linear relation between UV and [C II] luminosity is shown as the black line with 1σ uncertainties as blue and salmon coloured bands for the fit to M_{UV} and $M_\star$, respectively. The fainter band is the relation when including intrinsic dispersion around the mean relation, which is found to be $\sigma_{\mathrm{UV}} = 0.42 \pm 0.17$ for the upper panel, and $\sigma_{\mathrm{M}_\star} = 0.39 \pm 0.17$ dex for the lower one (see text for details).

that quantity with respect to [C II] luminosity. The first method uses the UV LF and a relation between L_{UV} and $L_{[\mathrm{C\,II}]}$ to build the [C II] LF. Similarly, our second method uses the SMF from A. Weibel et al. (2024) and converts it into a [C II] LF using the $M_\star$–$L_{[\mathrm{C\,II}]}$ relation we derived. In the following sections, we will refer to these two methods as UV-LF-based and SMF-based methods, respectively. In the third method, we derive step-wise estimates of the [C II] LF following the approach used for the ALPINE sample in L. Yan et al. (2020).

3.1 Empirical modelling based on the L_{UV}-$L_{[\mathrm{C\,II}]}$ relation

The first method to derive the [C II] LF relies on the UV LF from R. J. Bouwens et al. (2021) and an empirical relation between the UV and [C II] luminosities. The first step is to derive the L_{UV}-$L_{[\mathrm{C\,II}]}$ relation including the intrinsic dispersion. In both cases, we use our SED fitting results to derive the UV luminosities at 1500 Å. The upper panel of Fig. 2 shows the L_{UV}-$L_{[\mathrm{C\,II}]}$ relation for both the REBELS sources at $z \sim 7$ and for the ALPINE sample at $z \sim 5$. As can be seen, at fixed UV luminosity, the two samples show a very similar mean [C II] luminosity and scatter. This is perhaps not surprising, since the relation between SFR and $L_{[\mathrm{C\,II}]}$ has been shown to show little evolution from the local Universe out to $z \sim 6$, likely continuing out to $z \sim 8$ (see e.g. J. Matthee et al. 2019; D. Schaerer et al. 2020, S. Schouws et al., in preparation).

In order to increase the dynamic range in our modelling of the L_{UV}-$L_{[\mathrm{C\,II}]}$ relation, we consider both the ALPINE and REBELS samples. The computation of the Spearman coefficient for the total sample shows a weak monotonicity and correlation between the parameters with a value of 0.28 and a p-value of 0.005. For the REBELS detections, this coefficient falls to $\rho = -0.04$. We can therefore not use this sample alone, mostly due to its narrow range spanned in UV ($\Delta M_{\mathrm{UV}} \sim 1.5$ mag versus ∼3 mag for ALPINE). We thus include the combined sample of ALPINE and REBELS sources assuming they trace similar representative galaxy populations at high-redshift.

The best-fitting relation between the [C II] and UV luminosities is modelled using the python implementation[2] of the LINMIX package (B. C. Kelly 2007). This is used to perform a Bayesian linear regression with uncertainties in both L_{UV} and $L_{[\mathrm{C\,II}]}$, including upper limits. Only the ALPINE upper limits will be considered (see Section 2).

We thus derive the linear relation between L_{UV} and $L_{[\mathrm{C\,II}]}$ allowing for an intrinsic Gaussian dispersion (σ_{UV}) around the mean relation:

$$\log(L_{[\mathrm{C\,II}]}/\mathrm{L}_\odot) = a_{\mathrm{UV}} + b_{\mathrm{UV}} \times \log(L_{\mathrm{UV}}/\mathrm{L}_\odot) + \sigma_{\mathrm{UV}}. \quad (1)$$

In this equation, we use $L_{\mathrm{UV}} = \nu L_\nu$, evaluated at rest-frame 1500 Å. The posterior mean values and their 1σ uncertainties of the different parameters are $a_{\mathrm{UV}} = -4.49 \pm 2.01$, $b_{\mathrm{UV}} = 1.18 \pm 0.19$, and $\sigma_{\mathrm{UV}} = 0.42 \pm 0.17$. This is also shown in Fig. 2. As a test we also fit the relation to the REBELS sample alone, fixing the slope to the $b_{\mathrm{UV}} = 1.18$ value and leaving the normalization free. This leads to +0.15 dex offset above the combined relation, well within σ_{UV}. Additionally, while there is some uncertainty as to the nature of those sources in REBELS whose spectral scans did not yield a [C II] detection, if we assume this is due to their line being too faint for detection, this only impacts a small fraction of the sources in our total fits, resulting in <0.1 dex lower $L_{[\mathrm{C\,II}]}$-M_{UV} (or M_*) relation. When compared to other issues we will discuss (e.g. UV LF versus SMF-based determinations), the impact of this issue is relatively small and will be ignored in the discussion which follows.

With this relation in hand, we can now derive the [C II] LF, based on the known $z \sim 7$ UV LF from R. J. Bouwens et al. (2021). We adopt the Schechter parametrization of the $z \sim 7$ UV LF from R. J. Bouwens et al. (2021). Out to $M_{\mathrm{UV}} \sim -23$, the brightest magnitudes probed by REBELS, the Schechter and double-power-law fits (from R. A. A. Bowler et al. 2020; R. J. Bouwens et al. 2021, respectively) agree within the uncertainties of the two parametrizations, so the choice has a negligible effect on the resulting [C II] LF.

In order to compute uncertainties, we adopt a Monte Carlo approach. We sample 500 000 points from the UV LF and convert

[2] https://github.com/jmeyers314/linmix

Downloaded from academic.oup.com/mnras/article/553/2/stag2017/8994297 by Liverpool John Moores University user on 16 November 2026

Table 1. [C II] LF parameters derived from Schechter function fits at $z \sim 5$ and $z \sim 7$.

Method	Redshift	$\log \phi^*_{[\mathrm{C\,II}]}$	$\log L^*_{[\mathrm{C\,II}]}$	$\alpha_{[\mathrm{C\,II}]}$
UV LF	$z \sim 7$	$-4.71^{+0.40}_{-0.30}$	$9.04^{+0.15}_{-0.16}$	$-2.04^{+0.10}_{-0.11}$
SMF	$z \sim 7$	$-4.50^{+0.91}_{-0.23}$	$9.11^{+0.11}_{-0.27}$	$-2.41^{+0.14}_{-0.11}$
SMF	$z \sim 5$	$-4.20^{+0.67}_{-0.23}$	$9.25^{+0.15}_{-0.22}$	$-2.34^{+0.12}_{-0.10}$

Note. $\phi^*_{[\mathrm{C\,II}]}$ is in $\mathrm{Mpc^{-3}dex^{-1}}$ and $L^*_{[\mathrm{C\,II}]}$ in $\mathrm{L_\odot}$.

their corresponding L_{UV} values to $L_{[\mathrm{C\,II}]}$, using equation (1) and the intrinsic dispersion σ_{UV}. Finally, we fit a Schechter function (P. Schechter 1976) to the resulting $L_{[\mathrm{C\,II}]}$ values, which in logarithmic form reads

$$\phi(\log L)\,\mathrm{d}\log L = \ln(10)\,\phi^*\,10^{(\alpha+1)(\log L - \log L^*)} \times \exp\left(-10^{\log L - \log L^*}\right)\mathrm{d}\log L, \quad (2)$$

with the three parameters ϕ^*, L^*, and α, representing the normalization, the characteristic luminosity, and the faint-end slope of the [C II] LF, respectively.

This procedure is repeated 10^4 times, varying the input Schechter parameters of the UV LF according to the appropriate covariance matrix from R. J. Bouwens et al. (2021). This procedure results in 10^4 [C II] LFs, from which the mean and standard deviation for all three Schechter parameters are computed. The resulting values are listed in Table 1.

3.2 Empirical modelling based on the $M_\star$-$L_{[\mathrm{C\,II}]}$ relation

The second method is effectively the same as the first albeit with different ingredients. Here, we derive the [C II] LF using the $z \sim 7$ SMF from A. Weibel et al. (2024)[3] and an empirical relation between stellar mass and [C II] luminosity. We derive the $M_\star$-$L_{[\mathrm{C\,II}]}$ along with its intrinsic dispersion using the same tool and sample as in Section 3.1. The empirical relation is shown in the lower panel of Fig. 2, and follows:

$$\log(L_{[\mathrm{C\,II}]}/\mathrm{L_\odot}) = \mathrm{a_{M_\star}} + \mathrm{b_{M_\star}} \times \log(\mathrm{M_\star/M_\odot}) + \sigma_{\mathrm{M_\star}}. \quad (3)$$

The Spearman coefficient shows a stronger correlation between $M_\star$ and [C II] luminosity compared to UV luminosity, with a value of 0.56 and a p-value of 2×10^{-9}. We also find a positive correlation using the REBELS sample alone $\rho = 0.39$ but with a lower confidence $p = 0.04$ and with much larger uncertainties on the slope.

The posterior mean values of the LINMIX fit and their 1σ uncertainties of the different parameters are $a_{M_\star} = 2.46 \pm 0.93$, $b_{M_\star} = 0.61 \pm 0.09$, and $\sigma_{M_\star} = 0.39 \pm 0.17$. As in Section 3.1, we fit the relation using the REBELS sample alone at the fixed slope of the combined sample leading to a $+0.23$ dex offset again attributed to the exclusion of non-detections from our fits and uncertainties associated with that (see Section 3.5 for implications on the resulting [C II] LF). Similarly, we derive the [C II] LF using that relation and the SMF at $z \sim 7$ from A. Weibel et al. (2024). We adopt the same Monte Carlo approach and sample points from the SMF and convert their $M_\star$ values into $L_{[\mathrm{C\,II}]}$ using the corresponding empirical relation. The results are listed in Table 1. Additionally, we repeat the same analysis at $z \sim 5$. We use the SMF from A. Weibel et al. (2024) at the $z \sim 5$ in order to derive the [C II] LF appropriate for a comparison with the ALPINE sample. The $z \sim 5$ Schechter parameters for the resulting [C II] LF are also listed in Table 1.

[3]We convert all stellar masses in the REBELS and ALPINE catalogues from a Chabrier IMF to a Kroupa IMF using the usual 0.05 dex correction in order to use the SMF from A. Weibel et al. (2024).

3.3 Step-wise estimate based on the REBELS [C II] sample

In our third approach, we derive step-wise [C II] LFs, closely following the method developed in L. Yan et al. (2020) for the derivation of the [C II] LF from the ALPINE sample [see also L. Barrufet et al. 2023b, where the same approach is used to estimate the infrared (IR) LF].

As in the first approach, we use the $z \sim 7$ UV LF from R. J. Bouwens et al. (2021) as the reference to derive a representative volume for individual galaxies. In particular, we derive the total number of expected galaxies in a volume limited survey and compare this to the number of galaxies that are actually targeted by REBELS. The expected number of galaxies in a given bin $\mathrm{M_{UV}} \pm \Delta\mathrm{M_{UV}}/2$ is given by

$$N_{\mathrm{exp}} = \phi_{\mathrm{UV}}(M_{\mathrm{UV}})\,\Delta M_{\mathrm{UV}}\,V_{\mathrm{tot}}, \quad (4)$$

where ϕ_{UV} is the UV LF (expressed in units of $\mathrm{mag^{-1}}$), and V_{tot} is the total survey volume over which REBELS sources were selected. While we assume an area of 7 $\mathrm{deg^2}$ and $z = 6.4$-7.7 in computing V_{tot}, normalization of the [C II] LF is done using the UV LF, and thus the final result will not be sensitive to the assumed survey volume.

REBELS only targeted the brightest galaxies in the rest-UV identified over a 7 $\mathrm{deg^2}$, where tight constraints could be set on the redshift likelihood distribution. We can derive the 'completeness' factor in each UV luminosity bin as $f_{\mathrm{UV}} = N_{\mathrm{exp}}/N_{\mathrm{obs}}$, where N_{obs} is the number of targeted REBELS galaxies in the given bin.

The requirement for a $>4\sigma$ [C II] line detection in our target sample introduces a reduction in the survey volume for each source, which can be accounted for using the available volume V_{max} factor (see M. Schmidt 1968). For each source, we thus compute the maximum redshift up to which it would be detected at $>4\sigma$.

We now have all quantities to calculate the [C II] LF $\phi_{[\mathrm{C\,II}]}$ in bins of $L_{[\mathrm{C\,II}]}$. This is given by

$$\phi_{[\mathrm{C\,II}]} = \frac{1}{\Delta \log L} \sum_{i \in \mathrm{bin}} \frac{f_{\mathrm{UV},i}}{V_{\mathrm{max},i}}, \quad (5)$$

where $\Delta \log L$ is the logarithmic width of the bins, i runs over all sources in a given [C II] luminosity bin, and $V_{\mathrm{max,i}}$ is the maximum comoving volume of each source (see equation 3 in L. Yan et al. 2020). The above equation is also used to derive the appropriate Poisson uncertainties for each LF bin. The resulting [C II] LF step-wise results are shown in Fig. 3 as well as Table 2.

3.4 Comparison of methods

The mean Schechter functions from the empirical modelling methods as well as the step-wise estimates and their respective uncertainties are shown on the lower panel of Fig. 3. To compare our methods and the implied number densities at each luminosity, we also show the ratio of both empirical methods in the top panel.

Overall, both our SMF-based method and UV-LF-based empirical modelling methods agree very well with one another

Downloaded from academic.oup.com/mnras/article/553/2/stag2017/8994297 by Liverpool John Moores University user on 16 November 2026

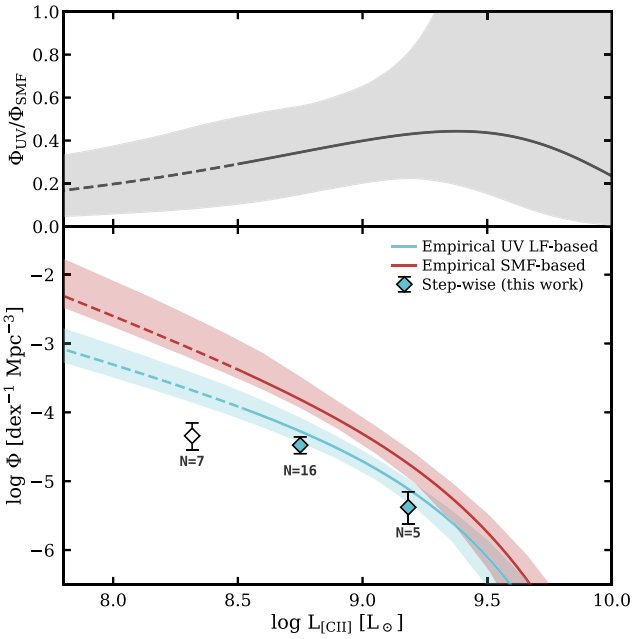


Figure 3. Comparison of the different methods used in this work to estimate the [C II] luminosity function at $z \sim 7$. The lower panel shows both empirical modelling methods with solid lines. The Schechter fit to the method using the UV luminosity function from R. J. Bouwens et al. (2021) and the empirical M_{UV}-$L_{[C\,II]}$ is shown in sky blue. The method using the SMF from A. Weibel et al. (2024) and the empirical $M_\star$-$L_{[C\,II]}$ relation is shown in dark red. We show 1σ contours for both methods as well as indicate incompleteness due to our M_{UV} selection with a dashed line below $\log(L_{[C\,II]}/L_\odot) = 8.5$. Sky blue diamonds show the step-wise method adapted from the method developed in L. Yan et al. (2020) with empty symbols below the completeness limit. We indicated the number of sources N in each $L_{[C\,II]}$ bin. The ratio between the UV LF and SMF-based methods is shown as a function of $\log L_{[C\,II]}$ on the upper plot in black.

Table 2. Step-wise [C II] LF at $z \sim 7$.

$\log L_{[C\,II]}$	N	$\log \phi$
[8.10-8.53]	7	$-4.34^{+0.19}_{-0.20}$
[8.53-8.97]	16	$-4.48^{+0.12}_{-0.12}$
[8.97-9.40]	5	$-5.38^{+0.23}_{-0.24}$

Note. $L_{[C\,II]}$ is in $L_\odot$ and ϕ in $Mpc^{-3}\,dex^{-1}$. Three equal-width bins over $8.1 \leq \log L_{[C\,II]}/L_\odot \leq 9.4$ ($\Delta \log L = 0.433$ dex), corresponding to the range of $L_{[C\,II]}$ measurements of REBELS. The number and width of bins were chosen to have $N > 4$ sources per bin. Uncertainties are 1σ Poisson.

at the bright end but display an increasingly large offset at $\log(L_{[C\,II]}/L_\odot) < 9$ reaching ~0.5 dex at $\log(L_{[C\,II]}/L_\odot) = 8.5$. We will refrain from drawing any significant conclusions based on the inferred [C II] LF at $\log(L_{[C\,II]}/L_\odot) < 8.5$ due to the initial M_{UV} cut of our sample (see Section 3.5). Because our sample is UV-selected, the inferred [C II] LF is biased against galaxies that are massive but UV-faint. If we assume that the SMF-based [C II] LF captures the totality of [C II] emitters, then the ratio of the SMF-based to the UV LF-based [C II] LF quantifies the fraction of [C II] emitters missed by UV-based selection alone. At $\log(L_{[C\,II]}/L_\odot) = 9$, the UV-based method recovers only 40 per cent of the sources captured by the SMF-based method, decreasing to 29 per cent at $\log(L_{[C\,II]}/L_\odot) = 8.5$. We therefore interpret the difference between the two methods as a measure of UV-selection incompleteness, implying that UV-based selections systematically underestimate the [C II] luminosity function.

As for the step-wise method, it shows good agreement with the UV-LF-based approach in the brightest two bins, increasing our confidence in the procedures used to derive those two results. However, the determination in the lowest luminosity bin at $\log L_{[C\,II]}/L_\odot < 8.5$ lies significantly below the derived Schechter function. This is most certainly due to the initial M_{UV} cut of the primary REBELS sample at $M_{UV} < -21.3$. At those magnitudes, the expected mean $\log L_{[C\,II]}/L_\odot$ is 8.3, according to our relation in equation (1). Hence, our input sample is missing galaxies with fainter UV luminosities that can still have [C II] luminosities up to $\log L_{[C\,II]}/L_\odot = 8.7$ including the 1σ intrinsic dispersion (see discussion in the next section).

As shown earlier, stellar mass exhibits a tighter correlation with $L_{[C\,II]}$ than UV luminosity does. In contrast, UV luminosity is strongly affected by dust attenuation and bursty star formation, introducing additional scatter in the L_{UV}–$L_{[C\,II]}$ relation. Moreover, UV-selected samples are intrinsically biased towards UV-bright systems. Such selections can miss massive, [C II]-luminous galaxies that are sufficiently UV-faint to fall below the detection threshold of REBELS-like surveys, while still contributing significantly to the total [C II] luminosity density. For these reasons, in the following sections and figures we interpret our UV-based determinations as lower limits on the true [C II] luminosity function at $z \sim 7$. In contrast, the SMF-based approach, is less affected by dust-selection biases and is therefore expected to provide a more complete census of [C II] emitters – and a closer estimate of the intrinsic [C II] luminosity function at this epoch.

3.5 Uncertainties and possible systematics

The accuracy of our analysis is dependent on the quality of the multiple ingredients used for estimating the [C II] LF, namely the samples used for the empirical relations as well as the validity of the UV LF and the SMF. Furthermore, these samples only provide us with a good probe of the [C II] LF over the range of luminosities and masses sampled by the observations. The luminosity bins we adopt for Schechter fits follow the distribution seen in our samples, but ultimately render the estimate at the upper and lowermost bins uncertain. This is due to the scatter in the empirical relations, leading to less reliable estimates of the number densities there. Furthermore, the faint-end slope $\alpha_{[C\,II]}$ of the Schechter fit is particularly sensitive to results in the lowest luminosity bin – where incompleteness can be an issue. Nevertheless, using our empirical relations, both the knee of the UV LF and the SMF should lie in the regime, where our sample is largely complete. This allows us to constrain both the normalization $\phi^*_{[C\,II]}$ and the knee $L^*_{[C\,II]}$ of the [C II] LF.

Another potential systematic comes from the normalization of the empirical relations. In Sections 3.1 and 3.2, we tried fitting the REBELS detections sample at fixed slope, which placed them +0.15 and +0.23 dex above the combined L_{UV}–$L_{[C\,II]}$ and $M_\star$–$L_{[C\,II]}$ relations, respectively. We note these are still within the intrinsic scatter of both relations fitted on the combined ALPINE and REBELS sample. Adopting these normalizations at fixed b and σ would translate the per-dex LF, $\phi'(\log L) = \phi(\log L - \Delta)$, raising $\log L^*_{[C\,II]}$ by the same amount Δ with $\phi^*_{[C\,II]}$ and $\alpha_{[C\,II]}$ left unchanged. We attribute this effect to REBELS sampling the

Downloaded from academic.oup.com/mnras/article/553/2/stag2017/8994297 by Liverpool John Moores University user on 16 November 2026

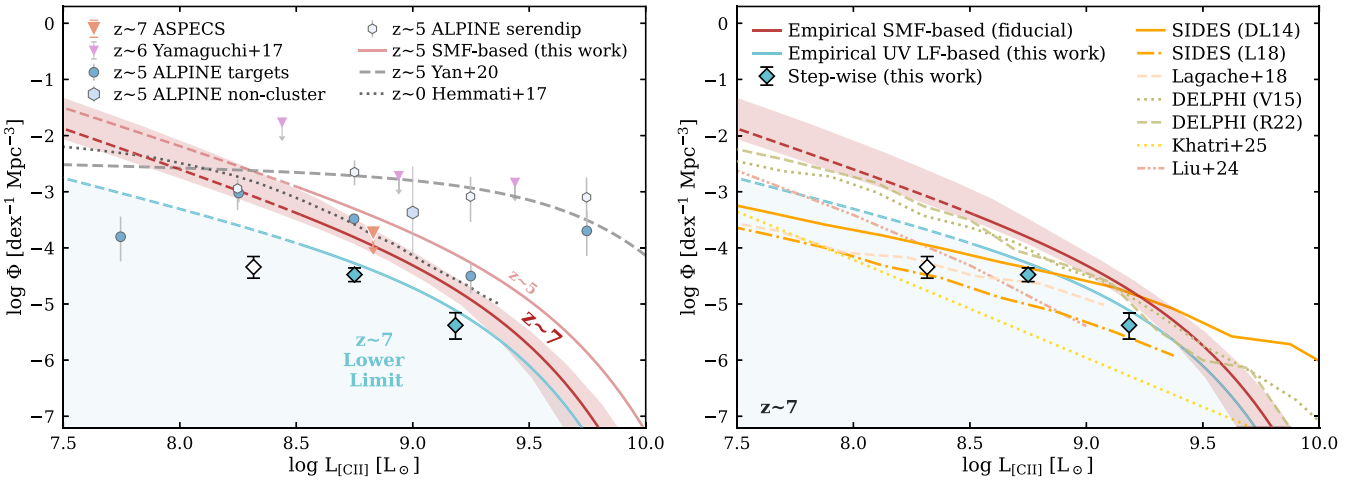


Figure 4. Comparison between [C II] luminosity function estimates from different observations (left) and various semi-analytical models and simulations (right). In both panels, the sky blue lines show the LFs from the UV-based method while the dark red lines show the SMF-based one; solid above $\log(L_{[\mathrm{C\,II}]}/\mathrm{L}_\odot) = 8.5$ and dashed below to indicate incompleteness due to our M_{UV} selection. As the UV-LF-based method may miss a certain fraction of [C II] emitters (see Section 4.4), it is shown as a lower limit on both panels. We show the step-wise estimate based on the UV LF as filled blue diamonds and empty symbols below the completeness limit. **Left:** We show the measured [C II] LF at $z \sim 0$ (S. Hemmati et al. 2017) and limits at $z \sim 7$ from ASPECS (B. D. Uzgil et al. 2021) and at $z \sim 6$ (Y. Yamaguchi et al. 2017). The $z \sim$ 4-6 determinations from ALPINE are shown in blue circles for the target sample (L. Yan et al. 2020) and grey hexagons for the serendipitous sample including a large overdensity at $z = 4.5$ and in the general field (hexagon with dark grey outline; F. Loiacono et al. 2021). The grey dashed line shows the Schechter function for $z \sim 5$ derived in L. Yan et al. (2020) from a fit to a combination of ALPINE results and [C II] LF estimates derived from CO observations. Using the same SMF-based method but relying on the $z \sim 5$ SMF from A. Weibel et al. (2024), we derive an independent estimate of the [C II] LF at $z \sim 5$ (salmon line). Unsurprisingly, this is in agreement with the targeted sample. **Right:** We show simulated [C II] LFs at $z \sim 7$ from various theoretical works: the simulated LFs from the SIDES simulation in orange (M. Béthermin et al. 2022), using two different $L_{[\mathrm{C\,II}]}$–SFR relations (DL14 for I. De Looze et al. 2014) and (L18 for G. Lagache, M. Cousin & M. Chatzikos 2018), the G. Lagache et al. (2018, dashed peach) estimate at $z \sim 6.7$, P. Khatri, E. Romano-Díaz & C. Porciani (2025, dotted gold) from the MARIGOLD simulation, the fiducial result from analytical bursty star formation model of L.-J. Liu et al. (2024, dash–dotted pink) with $\epsilon_{\mathrm{ff}} = 0.015$ at $z \sim 7.5$ and the `Delphi` semi-analytical model in a dotted and dashed khaki lines (P. Dayal et al. 2014, 2022). The `Delphi` predictions, using either the L. Vallini et al. (2015) or M. Romano et al. (2022) relation (V15 and R22 in the figure, respectively), are the most consistent with our results.

upper side of the scatter with its higher detection floor in M_{UV} (and $M_\star$) and challenges associated with interpreting the [C II] non-detections.

Furthermore, while the $z \sim 7$ [C II] LF derived with the UV-based and step-wise methods agree well down to $\log(L_{[\mathrm{C\,II}]}/\mathrm{L}_\odot) = 8.5$, both remain lower limits for the reasons presented earlier: They cannot account for sources sufficiently obscured in the UV to escape REBELS-like selection, such as extreme sub-mm galaxies already known to exist at these redshifts (e.g. D. A. Riechers et al. 2017; D. P. Marrone et al. 2018).

It is worth noting that even in the REBELS survey itself, a population of 'normal' obscured galaxies at $z \sim 7$ has been unveiled. Y. Fudamoto et al. (2021) serendipitously found two galaxies as neighbours to two REBELS targets at $z \sim 7$. At face value, their number density is $\sim 10^{-4}$ Mpc^{-3} with [C II] luminosities of $\sim 8 \times 10^8$ L$_\odot$. After accounting for the clustering excess given that these two galaxies were found as neighbours to luminous targets, their expected [C II] LF is in excellent agreement with our SMF-based method. Nevertheless, the detection of these sources shows that there are some UV-faint, [C II]-bright galaxies that are missing from our analysis.

Similarly, the ALPINE primary sample certainly revealed some galaxies, which had exceptionally high [C II] luminosities but modest UV luminosities. One example is a source which has a [C II] luminosity in excess of $10^{9.5}$ L$_\odot$ but is nevertheless one of the faintest galaxies in the rest-UV in ALPINE (see Fig. 2). This source is responsible for the extremely high [C II] LF estimate in the ALPINE target at $\log(L_{[\mathrm{C\,II}]}/\mathrm{L}_\odot) = 9.75$, which lies almost one dex above the step-wise LF estimate in the next fainter bin (see Fig. 4).

Furthermore, the ALPINE serendipitous sample of F. Loiacono et al. (2021) illustrates how overdensities can inflate the inferred [C II] LF: 11 of their 12 serendipitous [C II] detections belong to a single large overdensity at $z = 4.5$ in the Cosmic Evolution Survey (COSMOS) field. F. Loiacono et al. (2021) address this by deriving separate 'field' and 'clustered' luminosity functions. The clustered points lie well above the field determination, which indicates that number densities in such regions are not representative of the cosmic average. This highlights the sensitivity of [C II] LF measurements to cosmic variance in small survey volumes. The field LF, however, rests on the single remaining galaxy outside the overdensity and is correspondingly uncertain. Nevertheless it is consistent within 1σ with the targeted sample from L. Yan et al. (2020) and with our derived $z \sim 5$ [C II] LF using the [C II]–UV luminosity relation.

In summary, the [C II] LFs we derived with both UV-based methods in the previous sections are most likely underestimated by some degree, possibly even in the highest luminosity bins, due to the proven existence of UV-faint galaxies with significant [C II] luminosities. We therefore adopt our SMF-based approach as the fiducial result of this paper, which therefore tries to account for UV-faint and dusty massive [C II] emitters. This determination is nevertheless not itself free of selections effects: It inherits the systematics of the input SMF, which carries uncertainties from SED-fitting and model assumptions, may incompletely recover red or dust-obscured galaxies, and is subject to cosmic variance in the

Downloaded from academic.oup.com/mnras/article/553/2/stag2017/8994297 by Liverpool John Moores University user on 16 November 2026

limited volumes from which it is derived. Mapping the intrinsic [C II] LF directly will ultimately require wider blind [C II] surveys at $z \sim 7$.

4 COMPARISONS WITH OTHER OBSERVATIONS AND THEORETICAL WORKS

4.1 Comparison with lower redshift results

In this section, we will compare our $z \sim 7$ LF estimates with other estimates from the literature. The most direct comparison can be made with the ASPECS analysis from B. D. Uzgil et al. (2021). In particular, ALMA SPECtroscopic Survey in the Hubble Ultra Deep Field (ASPECS) blindly scanned the full ALMA band 6 for line emitters over the HUDF, i.e. its scan covers the [C II] line at $z = 6$-8 (see also R. Decarli et al. 2020). While no serendipitous lines were found at high significance, the resulting upper limit on the [C II] LF is still quite constraining. As can be seen in Fig. 4, the upper limit is only ∼0.5 dex above our step-wise determination. Hence, the two measurements are fully consistent. The ASPECS upper limit lies essentially at the same level as the measured $z \sim 0$ [C II] LF from S. Hemmati et al. (2017) and 1σ above our fiducial [C II] LF of our SMF-based method.

The comparison to $z \sim$ 4-6 from the ALPINE survey is done in two steps. First, we discuss the 'total' Schechter function that was provided by L. Yan et al. (2020). This LF was derived from a fit to the serendipitous sources from F. Loiacono et al. (2021) without any correction for clustering, as well as to LF points derived from converting CO LFs to [C II]. As can be seen in Fig. 4, this fit does not really pass through the majority of the ALPINE targeted sample, having an extremely shallow faint-end slope. At $L_{[C\,II]} = 10^9$ L$_\odot$, this Schechter function is >1 dex higher than our $z \sim 7$ estimate (as well as the ALPINE targeted sample). This would indicate an extremely fast evolution across the ∼400 Myr from $z \sim 7$ to $z \sim 5$.

However, when deriving the $z \sim 5$ [C II] Schechter parameters in the same way as for the REBELS sample at $z \sim 7$ using the SMF from A. Weibel et al. (2024), we obtain a much more moderate evolution of only ∼0.5−0.6 dex across this redshift range and over the luminosities shown in Fig. 4. Our $z \sim 5$ Schechter function indeed passes through the step-wise estimates from the ALPINE targeted sample, except in the brightest and faintest bin, likely due to the UV-luminosity cut in the input sample (similar to REBELS). At the bright end, the step-wise estimate is significantly boosted by one particular galaxy that is very faint in UV luminosity, but [C II] luminous. Its faint UV luminosity results in a very high f_{UV} factor, thus boosting the brightest LF point. Nevertheless, we consider our $z \sim 5$ Schechter function derivation as more representative of the ALPINE targeted sample, indicating a much more gradual evolution from $z \sim 7$ to $z \sim 5$ and consistent with that seen in the UV LF.

Essentially, the shape of our [C II] LF is very similar to that of the $z \sim 0$ [C II] LF from S. Hemmati et al. (2017) and shows only mild evolution to $z \sim 5$. This is not especially surprising given that [C II] is an SFR-tracer and that we observe similar values for the SFRD at $z \sim 0$ and at $z =$ 5-7 (see Section 4.3 and Fig. 5).

4.2 Comparison with semi-analytical models and simulations

Fig. 4 also shows recent [C II] LF predictions from different theoretical studies at $z \sim 7$. These are all in reasonable agreement

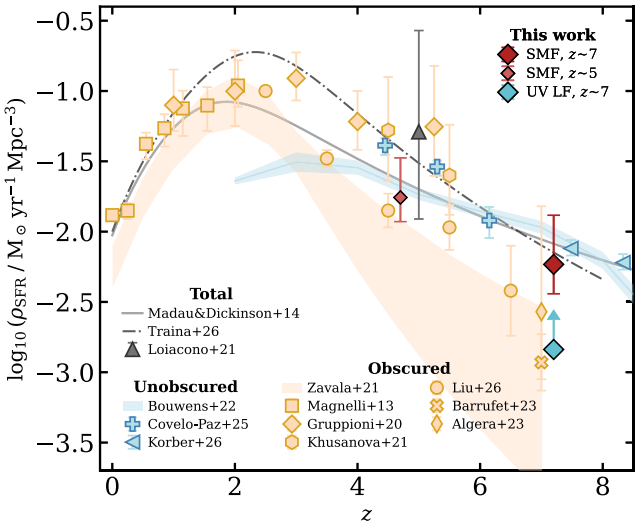


Figure 5. Cosmic star formation rate density as a function of redshift. Literature determinations are grouped by the star-formation tracer they probe – total (grey), unobscured (blue), and dust-obscured (tan) – while our [C II]-based results are shown as diamonds following the colour scheme of the previous figures. Our points at $z \sim 7$ are plotted with a slight offset for clarity. The UV-LF-based determination at $z \sim 7$ (sky blue diamond) is plotted as a lower limit (upward arrow), since UV-based determinations fail to account for the contribution from UV-faint galaxies (see Section 4.3). Our [C II]-derived values are obtained by integrating the corresponding [C II] LF down to $\log(L_{[C\,II]}/L_\odot) = 8.1$ (SFR ≈ 11 M$_\odot$ yr^{-1} using the I. De Looze et al. 2014 calibration). Total determinations (grey) comprise the parametric fits of P. Madau & M. Dickinson (2014) (solid) and A. Traina et al. (2026) (dash–dotted), and the [C II]-LF-based estimate from the ALPINE field sample (F. Loiacono et al. 2021, triangle). Unobscured tracers (blue) comprise the rest-UV SFRD of R. J. Bouwens et al. (2022b) (shaded band) and the nebular-line determinations from Hα (A. Covelo-Paz et al. 2025) and [O III] + Hβ (D. Korber et al. 2026; GLIMPSE). Like UV-selected samples, these recover star formation only in line-detected galaxies and miss heavily dust-obscured sources. Dust-obscured, IR-based determinations (tan) comprise J. A. Zavala et al. (2021) (shaded band), B. Magnelli et al. (2013), C. Gruppioni et al. (2020), Y. Khusanova et al. (2021), F.-Y. Liu et al. (2026), L. Barrufet et al. (2023b), and H. S. B. Algera et al. (2023). The convergence of our UV-LF-based lower limit with the obscured-only determinations at the bright end, together with the ∼0.5–0.7 dex offset from our fiducial SMF-based point, illustrates the contribution UV-faint, [C II]-bright systems make to the total SFRD at $z \sim 7$.

with the UV-based methods but in tension with our SMF-based procedure. Since we use a sample of galaxies at $z \sim$ 5-7 to calibrate the empirical relations, we also compute a $z \sim 6$ [C II] LF using the SMF at the same redshift from A. Weibel et al. (2024). A more direct comparison can be made with other theoretical works at $z \sim 6$ shown in Appendix A2.

First, G. Lagache et al. (2018) use a semi-analytical model of galaxy evolution combined with the photoionization code CLOUDY to predict the [C II] luminosity of galaxies at $z \sim 6.7$. The resulting [C II] LF has a relatively shallow slope, but it agrees with our step-wise results. While its normalization is below our lower limit, the bright end seems in agreement with our determinations from both UV- and SMF-based methods.

We show the model curves from M. Béthermin et al. (2022) estimated at $z \sim 7$, based on an updated version of the Simulated

Downloaded from academic.oup.com/mnras/article/553/2/stag2017/8994297 by Liverpool John Moores University user on 16 November 2026

Infrared Dusty Extragalactic Sky (SIDES) simulation.[4] The simulation predicts the [C II] LF based on two different conversions between SFR and [C II] luminosity. In the first approach, the 'standard' relation from I. De Looze et al. (2014) is used, which has also been shown to hold at higher redshifts (e.g. D. Schaerer et al. 2020). The second approach uses the relation from G. Lagache et al. (2018), which was calibrated with semi-analytical models and includes a redshift evolution in the conversion to account for lower metallicities. This predicts lower [C II] emission, resulting in a lower LF, as can also be seen in Fig. 4.

This comparison with the SIDES models is particularly interesting. All results from the SIDES simulations either are in agreement or lie below our lower limit to the [C II] LF (from the UV-based method) at the faint end. The bright end of all simulations show better agreement with our results. We note, however, that the simulation using the I. De Looze et al. (2014) relation has overall a more similar normalization across $L_{[\mathrm{C\,II}]}$ and redshift evolution as our results. This is consistent with the limited evolution seen in this conversion factor from the local Universe out to $z \sim 7$ (J. Matthee et al. 2019; D. Schaerer et al. 2020; see also S. Schouws et al., in preparation). Regarding the evolution from the presented $z \sim 6$ result in M. Béthermin et al. (2022) to $z \sim 7$, both uses of the SFR–$L_{[\mathrm{C\,II}]}$ relations from I. De Looze et al. (2014) and G. Lagache et al. (2018) relations show a 0.5 dex decrease from $z \sim 6$ to $z \sim 7$. A similar shift is seen using our method (see Appendix A2). Interestingly, this model also predicts an excess of objects with $L_{[\mathrm{C\,II}]} > 10^{9.5}$ $\mathrm{L}_\odot$, in tension with our fiducial determination. As discussed earlier, such luminous sources may still exist among UV-fainter galaxies missed by the current selection.

Additionally, we consider the results from P. Khatri et al. (2025) obtained from post-processing galaxies from the MARIGOLD cosmological simulation at redshifts $3 < z < 7$. Their double power-law relation sits well below our determination but nevertheless with a similar steepness on the faint-end slope.

We also consider comparisons against analytical model results of L.-J. Liu et al. (2024), which accounts for bursty star formation due to delayed supernova feedback. In this analytical model, $L_{[\mathrm{C\,II}]}$ scales with the gas mass and metallicity of each halo, and star formation bursts are driven by delayed supernova feedback, whose amplitude is set by the cloud-scale star formation efficiency ϵ_{ff}. We show their fiducial model ($\epsilon_{\mathrm{ff}} = 0.015$) at $z = 7.5$, the redshift closest to our sample. Similarly to other works, this model lies below our determination, however their $z \sim 6$ models are in good agreement with our results (see Appendix A2). The discrepancy seen here can be attributed to redshift evolution between $z \sim 7.5$ and our mean sample redshift of $z \sim 7$. We also note that their model results adopting instead $\epsilon_{\mathrm{ff}} = 0.005$ and 0.045 differ from their $\epsilon_{\mathrm{ff}} = 0.015$ results by only ∼0.2–0.4 dex over $8.5 < \log(L_{[\mathrm{C\,II}]}/\mathrm{L}_\odot) < 9.5$, which is less than the offset between our UV- and SMF-based determinations. Also, the effects of burstiness itself are concentrated at $\log(L_{[\mathrm{C\,II}]}/\mathrm{L}_\odot) \lesssim 8$, which is below our completeness limit and we therefore cannot discriminate between them. Nevertheless, all three model variants they present predict a similarly steep faint end slope, consistent with our $\alpha_{[\mathrm{C\,II}]} < -2$. Our data therefore cannot constrain the burstiness of star formation at $z \sim 7$, which will require deeper blind surveys or line intensity mapping.

[4] https://cesamsi.lam.fr/instance/sides/home

Finally, we compare to the `Delphi` semi-analytical model (P. Dayal et al. 2014, 2022), the latest version of which incorporates small-scale ISM physics calibrated on the `Sphinx` simulations (V. Mauerhofer et al. 2025). `Delphi` uses a binary merger-tree approach to jointly track the assembly of dark matter haloes and their gas, stellar, metal, and dust content, tuned with only two free parameters to reproduce the observed UV LF at high-redshifts with *JWST*. [C II] luminosities are then assigned to each galaxy using the SFR- and metallicity-dependent relation of L. Vallini et al. (2015, equation 8) and that of M. Romano et al. (2022). The [C II] LFs presented here are evaluated at $z \sim 6.4$-7.7. Of all the models considered here, `Delphi` most closely reproduces our fiducial (SMF based) [C II] LF, following it within the 1σ uncertainties in both shape and normalization across the observed luminosity range.

4.3 Implications for the SFRD

We make use of our fiducial [C II] LF to estimate the contribution from massive REBELS-like galaxies to the SFRD at $z \sim 7$. The SFRD is derived by integrating our [C II] luminosity function and applying the empirical [C II]–SFR calibration of I. De Looze et al. (2014) as follows:

$$\log\left(\frac{\rho_{\mathrm{SFR}}}{\mathrm{M}_\odot\,\mathrm{yr}^{-1}\,\mathrm{Mpc}^{-3}}\right) = -7.06 + \log\left(\frac{\rho_{[\mathrm{C\,II}]}}{\mathrm{L}_\odot\,\mathrm{Mpc}^{-3}}\right). \quad (6)$$

Uncertainties are propagated via Monte Carlo by drawing 10^4 samples from the MCMC posterior over $(\log\phi, \log L, \alpha)$, from which we report the median and 16th/84th percentile interval of $\log(\rho_{\mathrm{SFR}})$. In our case, $\alpha < -2$ would make the integral of the Schechter function diverge as $L_{\mathrm{min}} \to 0$ rendering the choice of L_{min} crucial. Given this and our uncertainty on the faint-end slope, we integrate down to $\log L_{\mathrm{min}}/\mathrm{L}_\odot = 8.1$ corresponding to the faintest [C II] detection in REBELS to avoid extrapolating the results below that directly observed with the probed sample. This corresponds to integrating down to an SFR of $11\,\mathrm{M}_\odot\,\mathrm{yr}^{-1}$.

We obtain $\log(\rho_{\mathrm{SFR}}/\mathrm{M}_\odot\,\mathrm{yr}^{-1}\mathrm{Mpc}^{-3}) = -2.23^{+0.35}_{-0.21}$ for the SMF-based method and $\log\rho_{\mathrm{SFR}}/\mathrm{M}_\odot\,\mathrm{yr}^{-1}\mathrm{Mpc}^{-3} = -2.84^{+0.21}_{-0.17}$ for the UV-based one. A direct comparison to other works is not meaningful, as they often use different integration limits depending on their SFR tracers and completeness. Nevertheless, the values we infer can be interpreted as the contribution from REBELS-like sources to the SFRD, as a fractional contribution to the total. Relative to the P. Madau & M. Dickinson (2014) fit at $z \sim 7$, our SMF-based value implies that massive, [C II]-bright galaxies comprise ∼63 per cent of the total SFRD at this epoch, with a comparable fraction obtained against the A. Traina et al. (2026) parametrization, which sits at a similar level at $z \sim 7$. As an indication, we also integrate our [C II] LF to a lower limit adopting the P. Madau & M. Dickinson (2014) convention, integrating here to $0.03L^*_{[\mathrm{C\,II}]}$, corresponding to $\log L_{\mathrm{min}}/\mathrm{L}_\odot = 7.6$. We obtain a value of $\log\rho_{\mathrm{SFR}}/\mathrm{M}_\odot\,\mathrm{yr}^{-1}\mathrm{Mpc}^{-3} = -1.87^{+0.40}_{-0.25}$, which is consistent within errors to P. Madau & M. Dickinson (2014). As the [C II] LF suggests, ρ_{SFR} at $z \sim 7$ is similar to that of the local Universe at $z \sim 0$ (S. Hemmati et al. 2017).

Other works have estimated the obscured contribution to the SFRD from IR tracers (B. Magnelli et al. 2013; C. Gruppioni et al. 2020; Y. Khusanova et al. 2021; J. A. Zavala et al. 2021; F.-Y. Liu et al. 2026), showing that the SFRD is dominated by obscured star formation up to $z \sim 5$–7. More recently, other works based on REBELS have estimated that obscured star formation accounts

Downloaded from academic.oup.com/mnras/article/553/2/stag2017/8994297 by Liverpool John Moores University user on 16 November 2026

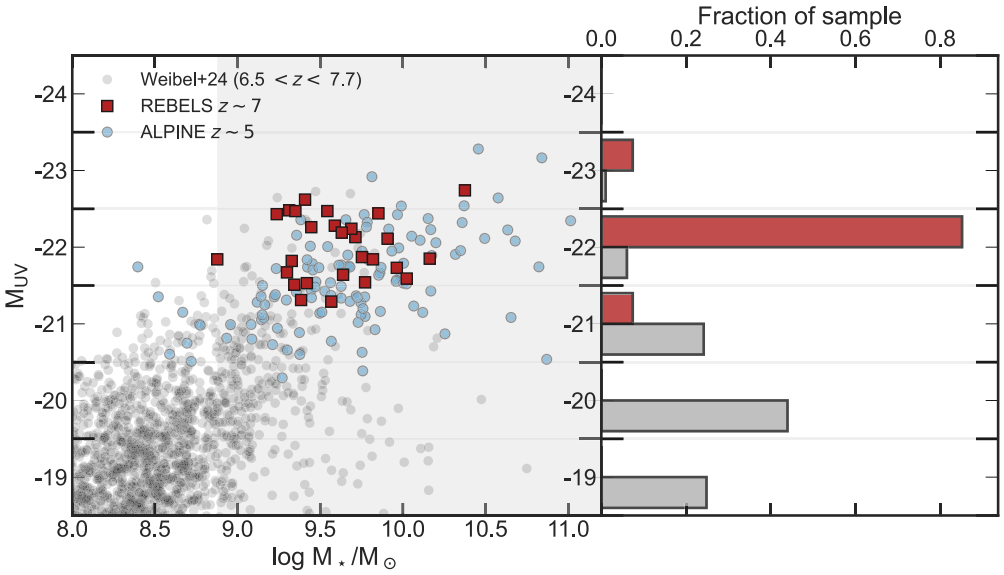


Figure 6. Distribution of sources in the $M_{\rm UV}$-$M_\star$ plane highlighting the differences in the samples used in this work. The SMF used for our empirical method is from A. Weibel et al. (2024), we plot the sources from their catalogue, within the redshift range of REBELS sources ($6.5 < z < 7.7$), as grey dots. REBELS sources are shown as red squares and ALPINE detections are also shown for reference as blue dots. This plot highlights the bias of both latter samples towards massive and UV-bright galaxies. The mass range probed by REBELS is shown as the grey shaded area. Fractions of the total sample in each $M_{\rm UV}$ bin in this mass range are shown on the right. REBELS sources and sources from A. Weibel et al. (2024) are shown in red and grey, respectively, in $\Delta M_{\rm UV} = 1$-mag bins of UV luminosity.

for 30 per cent of the cosmic SFRD at $z \sim 7$ (H. S. B. Algera et al. 2023; L. Barrufet et al. 2023b). These works focus on the obscured star formation occurring inside UV-selected sources and dark companions. In our case, the ratio between the SFRD from the SMF-based and UV-based methods does not correspond to the obscured fraction, but can instead be interpreted as the fraction of SFRD hosted by UV-faint systems missed by ALPINE and REBELS-like selections, hence does not include the star formation hosted by UV-bright galaxies themselves. By construction, that contribution comes from [C II] bright and therefore star-forming sources, which are massive but UV-faint, hence heavily dust-obscured. Their contribution should be quantified and added to the estimation from IR measurements to completely account for the SFRD at high redshift. The tension between different IR censuses underscores a remaining systematic uncertainty, however all approaches agree that the obscured/UV-faint contribution to the SFRD is still significant at $z \sim 7$.

4.4 Possible explanation for discrepancies

In summary, our $z \sim 7$ [C II] luminosity function lies in agreement with the ASPECS blind upper limits and aligns with the $z \sim 0$ relation, suggesting a moderate evolution in the number density of [C II] emitters with cosmic time. The UV-based result using the UV LF from R. J. Bouwens et al. (2021) and hence the REBELS sample likely underestimates the true abundance of [C II] emitters, missing the contribution from UV-faint and dust-obscured galaxies. In contrast, our SMF-based determination, which traces the underlying stellar mass distribution, yields higher number densities, and aligns well with the ALPINE targeted sample at $z \sim 5$, indicating a smooth evolution from $z \sim 7$ to $z \sim 5$ of $\sim +0.3$ dex in $\phi^*_{\rm [C\,II]}$, and to an overall $\sim$0.5 dex increase in number density at $\log(L_{\rm [C\,II]}/{\rm L}_\odot) > 8.5$. While the 'total' ALPINE fit of L. Yan et al. (2020) likely overestimates the bright end of the [C II] LF, it nevertheless highlights a physically important component: The contribution of companion galaxies detected serendipitously in the ALPINE pointings, which were not part of the UV-selected target list and would largely be missed by UV selection alone. These comparisons therefore suggest that the true [C II] LF likely lies above the UV-based estimate, with dusty, massive, and companion sources providing a non-negligible fraction of the [C II] luminosity density at early epochs. Our SMF-based determination is designed to recover this missing population, and we adopt it as our fiducial estimate of the intrinsic [C II] LF at $z \sim 7$.

The [C II] LFs from all models are in qualitative agreement with our determinations. Interestingly, while no model sits at the same normalization as our fiducial result, they are all broadly consistent with a steep faint-end slope. Most importantly, these other results do not suggest that we are missing a large number of extremely luminous [C II] emitters at $z \sim 7$ in the REBELS sample (except for the result from B. Yue & A. Ferrara 2019 and the SIDES simulation, see Appendix A2 at $z \sim 6$). However, all models underestimate the number densities of [C II] emitters overall and are in better agreement with or below our UV-LF-based determination. Our SMF-based [C II] LF suggests that a non-negligible fraction of $z \sim 7$ [C II] emitters are dusty, UV-faint galaxies, and that these sources account for the difference between the UV-based and SMF-based [C II] LFs shown in Fig. 3.

Furthermore, as shown in Fig. 6, a large proportion of massive ($M_\star \gtrsim 10^9\,{\rm M}_\odot$) galaxies are still UV-faint ($M_{\rm UV} > -21$), as per A. Weibel et al. (2024)'s catalogue of >30 000 sources across the main *JWST* fields. Starting from the A. Weibel et al. (2024)'s catalogue, we can also apply the $M_\star$-$L_{\rm [C\,II]}$ relation we derive in Section 3.2 and take the REBELS survey as a point of comparison. In REBELS redshift range of $6.5 < z < 7.7$, there are 159 galaxies

Downloaded from academic.oup.com/mnras/article/553/2/stag2017/8994297 by Liverpool John Moores University user on 16 November 2026

with $\log L_{[\mathrm{C\,II}]}/\mathrm{L}_\odot > 8.12$, i.e. the faintest [C II] detected with REBELS. However, only 17 of those sources have $M_{\mathrm{UV}} < -21.3$, i.e. the lower range of REBELS' absolute UV magnitudes. Under these assumptions, this implies that up to ∼90 per cent of bright [C II] sources could be missed by a UV-selected survey like REBELS. The differences in numbers of sources observed here are consistent with the 0.5–1.0 dex difference between our UV-LF-based and SMF-based results across [C II] luminosities above $\log(L_{[\mathrm{C\,II}]}/\mathrm{L}_\odot) > 8.0$.

Recent *JWST* results have confirmed that a substantial fraction of the massive galaxy population at $z > 6$ is heavily dust-obscured and therefore underrepresented in UV-selected samples (e.g. L. Barrufet et al. 2023a; I. Labbé et al. 2023), representing as much as ∼45 per cent at $z \sim 6$-8 of the integrated stellar mass density at $\log(M_\star/\mathrm{M}_\odot) \gtrsim 9.25$ (R. Gottumukkala et al. 2024). In addition, lower mass systems with high SFRs can also populate high $L_{[\mathrm{C\,II}]}$ bins. Overall, these findings indicate that a large proportion of [C II] emitters at high redshift likely remains undetected even in current deep ALMA follow-ups, highlighting the need for future wide-area, blind [C II] surveys.

5 SUMMARY AND CONCLUSIONS

In this paper, we used the REBELS ALMA survey and its pilot programmes to derive, for the first time, the [C II] 158 μm line LF at $z \sim 7$. We leverage the 27 galaxies with a detected ($>4\sigma$) [C II] emission line in the redshift range $z = 6.4$-7.7. Because the REBELS sample relies on a UV-selection to identify luminous [C II]-emitting galaxies rather than making these identifications over a fixed volume, this complicates the determination of the [C II] LF.

We employ three complementary approaches to derive the [C II] LF using the UV LF and SMF at $z \sim 7$ as proxies. The first method relies on the empirical L_{UV}-$L_{[\mathrm{C\,II}]}$ relation derived here from the combined ALPINE and REBELS sample to transform the UV LF from R. J. Bouwens et al. (2021) into a [C II] LF. The second method is similar but uses an empirical $M_\star$-$L_{[\mathrm{C\,II}]}$ relation to transform the SMF from A. Weibel et al. (2024) to a [C II] LF. The empirical $M_\star$-$L_{[\mathrm{C\,II}]}$ relation exhibits a significantly tighter correlation (Spearman coefficient of 0.56 versus 0.28 for the L_{UV}-$L_{[\mathrm{C\,II}]}$). The third method derives a step-wise LF result by following L. Yan et al. (2020), using completeness corrections based on the UV LF.

At the bright end ($\log L_{[\mathrm{C\,II}]}/\mathrm{L}_\odot > 9$), all three methods are in good agreement, yielding a characteristic luminosity of $\log L_{[\mathrm{C\,II}]}/L_\odot \simeq 9.1$. At intermediate luminosities ($8.5 < \log L_{[\mathrm{C\,II}]}/\mathrm{L}_\odot < 9$), the SMF-based determination lies ∼0.5 dex above the UV-LF-based methods. This difference grows close to 1 dex at the faint end, where the step-wise estimate also fails, becoming increasingly incomplete due to the initial UV selection of the target sample and the scatter in the L_{UV}–$L_{[\mathrm{C\,II}]}$ relation. We interpret this offset as representing a population of dust-obscured sources, systematically missed by UV-selected samples, that none the less have significant [C II] luminosities. This population is not captured well by UV-LF-based method, so we treat our UV-LF-based result as a lower limit on the true [C II] LF at $z \sim 7$. We adopt the SMF-based method as our fiducial determination because stellar mass exhibits a tighter correlation with [C II] luminosity than UV luminosity according to our empirical relations, and because the SMF is less biased against dust-obscured systems.

Comparing our $z \sim 7$ results with the ALPINE survey at $z \sim 5$, we find a moderate evolution in the normalization of ∼0.3 dex over ∼400 Myr. Importantly, when we apply the same SMF-based methodology to derive a $z \sim 5$ [C II] LF using the A. Weibel et al. (2024) SMF, we obtain good agreement with the ALPINE targeted sample, validating our approach. This smooth evolution is consistent with the build-up of stellar mass and star formation rate density over this redshift range (e.g. R. J. Bouwens et al. 2015; S. L. Finkelstein et al. 2015; R. A. A. Bowler et al. 2020; R. J. Bouwens et al. 2021; M. Stefanon et al. 2021), and contrasts with the steeper evolution that would be inferred from the serendipitous ALPINE sample. Intriguingly, our $z \sim 7$ determination is in excellent agreement with the $z \sim 0$ [C II] LF from S. Hemmati et al. (2017), which shows a remarkable consistency with the build-up of the cosmic star formation rate density over the same epoch.

Theoretical predictions are in qualitative agreement with our measurements. The `Delphi` model is in very good agreement with our result at $z \sim 7$ with either the L. Vallini et al. (2015) or M. Romano et al. (2022) relations. The SIDES simulation using the I. De Looze et al. (2014) SFR–$L_{[\mathrm{C\,II}]}$ relation also shows a similar evolution from $z = 6$ to $z = 7$, and the existence of populations of similarly [C II] bright sources at these redshifts.

However, all models systematically underpredict the number densities of [C II] emitters relative to our fiducial SMF-based results, sometimes compensating by predicting the existence of populations of extremely bright [C II]-emitters. Furthermore, the existence of at least one UV-faint galaxy with $\log L_{[\mathrm{C\,II}]}/\mathrm{L}_\odot > 9.5$ at $z \sim$ 4-6 in the ALPINE galaxy sample and the serendipitous detection of dusty sources at $z \sim 7$ from REBELS (Y. Fudamoto et al. 2021; I. F. van Leeuwen et al. 2024) show that a UV-preselected galaxy sample almost certainly underestimates the [C II] LF to some degree. Using the A. Weibel et al. (2024) catalogue and our $M_\star$-$L_{[\mathrm{C\,II}]}$ relation, we estimate that up to ∼90 per cent of galaxies with $\log L_{[\mathrm{C\,II}]}/\mathrm{L}_\odot > 8.12$ (the faintest REBELS detection) have $M_{\mathrm{UV}} > -21.3$ and would thus be excluded from UV-bright samples like REBELS.

Assuming our [C II] LF derived from the SMF-based method captures the totality of [C II]-bright emitters, the difference between the UV-based and SMF-based methods suggests that 60 per cent to 70 per cent of sources with $\log(L_{[\mathrm{C\,II}]}/\mathrm{L}_\odot) > 8.5$ might be missed by focusing on most UV luminous galaxies and more than >80 per cent at lower luminosities. Thus large galaxy samples, using unbiased line scans over wider areas and also probing the immediate neighbourhoods around massive galaxies (e.g R. Decarli et al. 2017; Y. Fudamoto et al. 2021; I. F. van Leeuwen et al. 2024), will be needed to estimate the required completeness corrections.

Furthermore, when deriving the SFRD implied by our [C II] LF using the I. De Looze et al. (2014) calibration, we find that ∼63 per cent of the cosmic SFRD at $z \sim 7$ (P. Madau & M. Dickinson 2014) appears to originate from massive, [C II]-bright galaxies. Because [C II] traces the total (obscured plus unobscured) star formation of the galaxies it samples, the ∼0.6 dex offset between our SMF- and UV-based SFRDs shows the impact that UV selection can have on the inferred properties of massive galaxies at these redshifts. This population overlaps strongly with, but is not identical to, the dust-obscured population, and the derived offset here is our best estimate as to the likely lower limit on its contribution. The implied missed fraction sits at the upper end of current estimates underscoring the need to quantify the contribution of UV-faint, obscured galaxies to the SFRD at $z \sim 7$.

Our results provide critical constraints for upcoming [C II] intensity mapping experiments including TIME (G. Sun et al.

Downloaded from academic.oup.com/mnras/article/553/2/stag2017/8994297 by Liverpool John Moores University user on 16 November 2026

2021), EoR-Spec (N. F. Cothard et al. 2020), and CONCERTO (M. Béthermin et al. 2022), which probe the aggregate [C II] emission during reionization. Specifically, the predicted [C II] power spectra expected for these surveys vary significantly depending on the shape of the [C II] LF and its evolution at $z > 6$. Additionally, bursty star formation is expected to boost the faint end of the [C II] LF and distort the [C II] power spectrum (L.-J. Liu et al. 2024), precisely in the regime below the reach of current targeted surveys. To fully characterize the [C II]-emitting population at $z \sim 7$ – including UV-faint and companion sources – future surveys will require deeper wide-area blind [C II] line scans. Such observations will be essential to determine whether the discrepancy between UV- and SMF-based estimates reflects a genuine population of dust-obscured [C II] emitters or systematic uncertainties in various empirical scaling relations.

ACKNOWLEDGEMENTS

The authors want to thank all the team members of ASPECS and ALPINE for many stimulating discussions regarding the [C II] LF and [C II] measurements of distant galaxies in general. Special thanks go to Bade Uzgil and Fabian Walter, as well as Lin Yan, Michele Ginolfi, Daniel Schaerer, and Matthieu Bethermin.

This paper makes use of the following ALMA data: ADS/JAO.ALMA#2019.1.01634.L. ALMA is a partnership of ESO (representing its member states), NSF (USA), and NINS (Japan), together with NRC (Canada), MOST and ASIAA (Taiwan), and KASI (Republic of Korea), in cooperation with the Republic of Chile. The Joint ALMA Observatory is operated by ESO, AUI/NRAO, and NAOJ. This research further made use of ASTROPY,[5] a community-developed core Python package for Astronomy (Astropy Collaboration 2013, 2018), in addition to other freely available software.[6] This project made use of the PYSIDES library[7] (see M. Béthermin et al. 2022), funded from the European Research Council (ERC) under the European Union's Horizon 2020 research and innovation programme (grant agreement no. 788212), and with support from the Excellence Initiative of Aix-Marseille University-AMidex, a French 'Investissements d'Avenir.

PAO acknowledges support from the Swiss National Science Foundation grants 190079 and 207349. The Cosmic Dawn Center (DAWN) was funded by the Danish National Research Foundation under grant no. 140. HSBA gratefully acknowledges support from Academia Sinica through grant AS-PD-1141-M01-2. MA was supported by FONDECYT grant number 1252054, and gratefully acknowledges support from ANID Basal Project FB210003, ANID MILENIO NCN2024_112, and ANID + Vinculación Internacional + FOVI250261. AF and AP acknowledge support from the ERC Advanced Grant INTERSTELLAR H2020/740120. Generous support from the Carl Friedrich von Siemens-Forschungspreis der Alexander von Humboldt-Stiftung Research Award is kindly acknowledged (AF). YF acknowledges support from NAOJ ALMA Scientific Research Grant number 2020-16B. MS acknowledges support from the European Research Commission Consolidator Grant 101088789 (SFEER), from the CIDEGENT/2021/059 grant by Generalitat Valenciana, and from project PID2023-149420NB-I00 funded by MICIU/AEI/10.13039/501100011033 and by ERDF/EU. PD acknowledges support from the European Research Council's starting grant ERC StG-717001 ('DELPHI'), from the NWO grant 016.VIDI.189.162 ('ODIN') and the European Commission's and University of Groningen's CO-FUND Rosalind Franklin programme. HI acknowledges support from NAOJ ALMA Scientific Research Grant Code 2021-19A. HI acknowledges support from JSPS KAKENHI Grant Number JP19K23462. RS acknowledges support from an STFC Ernest Rutherford Fellowship (ST/S004831/1).

DATA AVAILABILITY

The data for this paper will be made available upon reasonable request to the first author. The underlying ALMA raw data are publicly available in the science archive and will be made available in reduced form by the REBELS collaboration.

REFERENCES

Algera H. S. B. et al., 2023, MNRAS, 518, 6142
Algera H. S. B. et al., 2026, MNRAS, 545, staf1897
Aravena M. et al., 2024, A&A, 682, A24
Astropy Collaboration, 2013, A&A, 558, A33
Astropy Collaboration, 2018, AJ, 156, 123
Bakx T. J. L. C. et al., 2020, MNRAS, 493, 4294
Barrufet L. et al., 2023a, MNRAS, 522, 449
Barrufet L. et al., 2023b, MNRAS, 522, 3926
Béthermin M. et al., 2020, A&A, 643, A2
Béthermin M. et al., 2022, A&A, 667, A156
Bouwens R. J. et al., 2015, ApJ, 803, 34
Bouwens R. J. et al., 2021, AJ, 162, 47
Bouwens R. J. et al., 2022a, ApJ, 931, 160
Bouwens R. J., Illingworth G., Ellis R. S., Oesch P., Stefanon M., 2022b, ApJ, 940, 55
Bowler R. A. A., Jarvis M. J., Dunlop J. S., McLure R. J., McLeod D. J., Adams N. J., Milvang-Jensen B., McCracken H. J., 2020, MNRAS, 493, 2059
Bowler R. A. A. et al., 2024, MNRAS, 527, 5808
Cameron A. J., Katz H., Rey M. P., Saxena A., 2023, MNRAS, 523, 3516
Capak P. L. et al., 2015, Nature, 522, 455
Carilli C. L., Walter F., 2013, ARA&A, 51, 105
Carniani S., Maiolino R., Smit R., Amorín R., 2018, ApJ, 854, L7
Cescon K. et al., 2026, MNRAS, 549, stag924
Cothard N. F. et al., 2020, J. Low Temp. Phys., 199, 898
Covelo-Paz A. et al., 2025, A&A, 694, A178
Curti M. et al., 2023, MNRAS, 518, 425
Dayal P., Ferrara A., 2018, Phys. Rep., 780–782, 1
Dayal P., Ferrara A., Dunlop J. S., Pacucci F., 2014, MNRAS, 445, 2545
Dayal P. et al., 2022, MNRAS, 512, 989
De Looze I. et al., 2014, A&A, 568, A62
Decarli R. et al., 2017, Nature, 545, 457
Decarli R. et al., 2020, ApJ, 902, 110
Dessauges-Zavadsky M. et al., 2020, A&A, 643, A5
Faisst A. L. et al., 2020, ApJS, 247, 61
Faisst A. L. et al., 2026, ApJ, 1004, 22
Ferrara A., Vallini L., Pallottini A., Gallerani S., Carniani S., Kohandel M., Decataldo D., Behrens C., 2019, MNRAS, 489, 1
Finkelstein S. L. et al., 2015, ApJ, 810, 71
Fisher R. et al., 2025, MNRAS, 539, 109
Fudamoto Y. et al., 2021, Nature, 597, 489
Fudamoto Y. et al., 2022, ApJ, 934, 144
Fujimoto S. et al., 2019, ApJ, 887, 107
Gallerani S., Pallottini A., Feruglio C., Ferrara A., Maiolino R., Vallini L., Riechers D. A., Pavesi R., 2018, MNRAS, 473, 1909
Ginolfi M. et al., 2020, A&A, 633, A90

[5] http://www.astropy.org
[6] https://github.com/jmeyers314/linmix
[7] https://cesamsi.lam.fr/instance/sides/home

Downloaded from academic.oup.com/mnras/article/553/2/stag2017/8994297 by Liverpool John Moores University user on 16 November 2026

Gottumukkala R. et al., 2024, MNRAS, 530, 966
Gruppioni C. et al., 2020, A&A, 643, A8
Harvey T. et al., 2025, ApJ, 978, 89
Hashimoto T. et al., 2019, PASJ, 71, 71
Heintz K. E., Watson D., Oesch P. A., Narayanan D., Madden S. C., 2021, ApJ, 922, 147
Heintz K. E. et al., 2023, A&A, 678, A30
Heintz K. E. et al., 2024, Science, 384, 890
Hemmati S., Yan L., Diaz-Santos T., Armus L., Capak P., Faisst A., Masters D., 2017, ApJ, 834, 36
Herard-Demanche T. et al., 2025, MNRAS, 537, 788
Herrera-Camus R. et al., 2015, ApJ, 800, 1
Herrera-Camus R. et al., 2025, A&A, 699, A80
Hodge J. A., da Cunha E., 2020, R. Soc. Open Sci., 7, 200556
Hollenbach D. J., Tielens A. G. G. M., 1999, Rev. Mod. Phys., 71, 173
Inami H. et al., 2022, MNRAS, 515, 3126
Katz H. et al., 2019, MNRAS, 487, 5902
Kelly B. C., 2007, ApJ, 665, 1489
Khatri P., Romano-Díaz E., Porciani C., 2025, A&A, 697, A174
Khusanova Y. et al., 2021, A&A, 649, A152
Korber D. et al., 2026, A&A, 708, A43
Labbé I. et al., 2023, Nature, 616, 266
Lagache G., Cousin M., Chatzikos M., 2018, A&A, 609, A130
Le Fèvre O. et al., 2020, A&A, 643, A1
van Leeuwen I. F. et al., 2024, MNRAS, 534, 2062
van Leeuwen I. F. et al., 2025, MNRAS, 542, 1388
Liu F.-Y. et al., 2026, MNRAS, 545, staf1961
Liu L.-J., Sun G., Chang T.-C., Furlanetto S. R., Bradford C. M., 2024, ApJ, 974, 175
Loiacono F. et al., 2021, A&A, 646, A76
Madau P., Dickinson M., 2014, ARA&A, 52, 415
Magnelli B. et al., 2013, A&A, 553, A132
Maiolino R. et al., 2015, MNRAS, 452, 54
Markov V., Gallerani S., Pallottini A., Sommovigo L., Carniani S., Ferrara A., Parlanti E., Di Mascia F., 2023, A&A, 679, A12
Markov V., Gallerani S., Ferrara A., Pallottini A., Parlanti E., Mascia F. D., Sommovigo L., Kohandel M., 2025, Nat. Astron., 9, 458
Marrone D. P. et al., 2018, Nature, 553, 51
Matthee J., 2025, Contemp. Phys., 66, 116
Matthee J. et al., 2019, ApJ, 881, 124
Mauerhofer V., Dayal P., Haehnelt M. G., Kimm T., Rosdahl J., Teyssier R., 2025, A&A, 696, A157
Pallottini A. et al., 2022, MNRAS, 513, 5621
Pizzati E., Ferrara A., Pallottini A., Sommovigo L., Kohandel M., Carniani S., 2023, MNRAS, 519, 4608
Popping G., Narayanan D., Somerville R. S., Faisst A. L., Krumholz M. R., 2019, MNRAS, 482, 4906
Ramos Padilla A. F., Wang L., van der Tak F. F. S., Trager S. C., 2023, A&A, 679, A131
Riechers D. A. et al., 2017, ApJ, 850, 1
Robertson B. E., 2022, ARA&A, 60, 121
Romano M. et al., 2022, A&A, 660, A14
Rowland L. E. et al., 2024, MNRAS, 535, 2068
Rowland L. E. et al., 2026, MNRAS, 546, staf2023
Sanders R. L., Shapley A. E., Topping M. W., Reddy N. A., Brammer G. B., 2024, ApJ, 962, 24
Schaerer D. et al., 2020, A&A, 643, A3
Schechter P., 1976, ApJ, 203, 297
Schmidt M., 1968, ApJ, 151, 393
Schouws S. et al., 2022, ApJ, 928, 31
Schouws S. et al., 2023, ApJ, 954, 103
Shivaei I. et al., 2026, A&A, 712, A132
Smit R. et al., 2018, Nature, 553, 178
Sommovigo L. et al., 2022, MNRAS, 513, 3122
Stacey G. J., Geis N., Genzel R., Lugten J. B., Poglitsch A., Sternberg A., Townes C. H., 1991, ApJ, 373, 423
Stanton T. M. et al., 2026, MNRAS, 547, stag449
Stark D. P., Topping M. W., Endsley R., Tang M., 2026, Encyclopedia of Astrophysics, Volume 4. Elsevier, Oxford, p. 453
Stefanon M., Bouwens R. J., Labbé I., Illingworth G. D., Gonzalez V., Oesch P. A., 2021, ApJ, 922, 29
Sun G. et al., 2021, ApJ, 915, 33
Topping M. W., Shapley A. E., Stark D. P., Endsley R., Robertson B., Greene J. E., Furlanetto S. R., Tang M., 2021, ApJ, 917, L36
Topping M. W. et al., 2022, MNRAS, 516, 975
Traina A. et al., 2026, A&A, 705, A255
Uzgil B. D. et al., 2021, ApJ, 912, 67
Vallini L., Gallerani S., Ferrara A., Pallottini A., Yue B., 2015, ApJ, 813, 36
Vallini L., Pallottini A., Ferrara A., Gallerani S., Sobacchi E., Behrens C., 2018, MNRAS, 473, 271
Vallini L. et al., 2024, MNRAS, 527, 10
Vallini L. et al., 2025, A&A, 700, A117
Weaver J. R. et al., 2023, A&A, 677, A184
Weibel A. et al., 2024, MNRAS, 533, 1808
Wolfire M. G., Hollenbach D., McKee C. F., Tielens A. G. G. M., Bakes E. L. O., 1995, ApJ, 443, 152
Wolfire M. G., Vallini L., Chevance M., 2022, ARA&A, 60, 247
Yamaguchi Y. et al., 2017, ApJ, 845, 108
Yan L. et al., 2020, ApJ, 905, 147
Yue B., Ferrara A., 2019, MNRAS, 490, 1928
Zanella A. et al., 2018, MNRAS, 481, 1976
Zavala J. A. et al., 2021, ApJ, 909, 165

APPENDIX A: ADDITIONAL TESTS AND COMPARISONS

A1 Other SMFs

We adopted the SMF from A. Weibel et al. (2024) for our fiducial [C II] LF estimation. We also show how the same derivation would have performed with the SMFs from M. Stefanon et al. (2021), J. R. Weaver et al. (2023), and T. Harvey et al. (2025) in Fig. A1 and Table A1. We favour A. Weibel et al. (2024) for the following reason. It is measured over four independent, contiguous *JWST*/NIRCam fields (CEERS-EGS, PRIMER-COSMOS, PRIMER-UDS and JADES-GOODS-S) spanning $\sim$500 arcmin^2 and $>$30 000 rest-optically selected galaxies reduced through a single homogeneous pipeline. This allows us to better control for field-to-field 'cosmic variance' while also incorporating fainter and redder objects missed by pre-*JWST* selections. Although the individual Schechter parameters differ owing to strong degeneracies between ϕ^*, L^*, and α, the resulting LFs agree within uncertainties over the luminosity range constrained by our data. Reassuringly, the fiducial [C II] LF we derive from A. Weibel et al. (2024) lies roughly near the middle of the [C II] LF results presented in Fig. A1.

Table A1. [C II] LF parameters derived from Schechter function fits at $z \sim 7$ using different SMFs from the literature.

SMF	Redshift	$\log \phi^*_{[\mathrm{C\,II}]}$	$\log L^*_{[\mathrm{C\,II}]}$	$\alpha_{[\mathrm{C\,II}]}$
S21	$z \sim 7$	$-4.73^{+0.27}_{-0.44}$	$9.17^{+0.15}_{-0.14}$	$-2.19^{+0.16}_{-0.24}$
W23	$z \sim 7$	$-2.92^{+0.29}_{-0.48}$	$9.12^{+0.26}_{-0.20}$	$-1.77^{+0.07}_{-0.11}$
H25	$z \sim 7$	$-5.98^{+0.37}_{-0.56}$	$10.17^{+0.51}_{-0.44}$	$-2.50^{+0.23}_{-0.31}$

Note. $\phi^*_{[\mathrm{C\,II}]}$ is in Mpc^{-3} dex^{-1} and $L^*_{[\mathrm{C\,II}]}$ in $L_\odot$. S21, W23, and H25, respectively, correspond to the SMFs presented in M. Stefanon et al. (2021), J. R. Weaver et al. (2023) and T. Harvey et al. (2025).

Downloaded from academic.oup.com/mnras/article/553/2/stag2017/8994297 by Liverpool John Moores University user on 16 November 2026

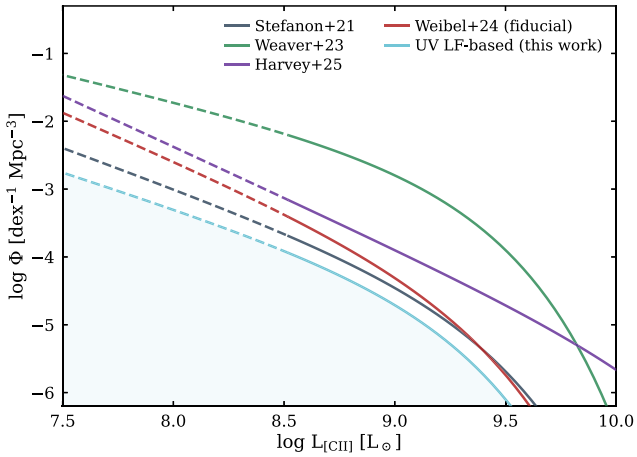


Figure A1. Comparison of the [C II] luminosity function at $z \sim 7$ derived using the empirical method and different SMFs from the literature. These estimates use M. Stefanon et al. (2021, dark blue), J. R. Weaver et al. (2023, green), T. Harvey et al. (2025, purple), and A. Weibel et al. (2024, red), with the latter adopted as our fiducial choice. The UV-LF-based estimate from this work is shown in blue. Solid lines indicate the luminosity range constrained by our data, while dashed lines show the extrapolation of our fit below the completeness threshold of our sample.

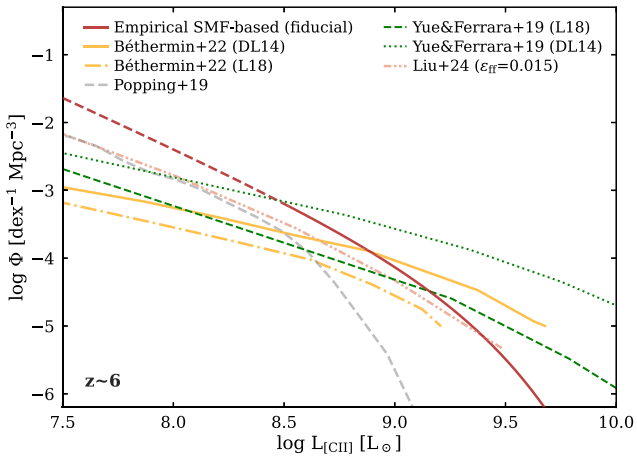


Figure A2. Theoretical predictions of the [C II] LF at $z \sim 6$. We show our SMF-based [C II] LF computed at $z \sim 6$ in red, that of G. Popping et al. (2019) in grey, B. Yue & A. Ferrara (2019) in green, the fiducial bursty model from L.-J. Liu et al. (2024) in pink, and the SIDES simulation in orange (M. Béthermin et al. 2022), using two different $L_{[C\,II]}$–SFR relations.

A2 Comparison with theoretical works at $z \sim 6$

To allow a fair comparison with other works, we also compute the [C II] LF using the SMF from A. Weibel et al. (2024) at $z \sim 6$ (Fig. A2). Several other theoretical predictions have been made at this redshift rather than at $z \sim 7$. Our empirical method, which is based on a sample of galaxies from $z \sim$ 4-8, should apply at $z \sim 6$. We can first compare with G. Popping et al. (2019), which combines a semi-analytical model of galaxy formation with chemical equilibrium networks and numerical radiative transfer models to derive the [C II] emission of galaxies at $z \sim 6$. Their results are consistent with our SMF-based method at the faint end, but this is primarily below the completeness limit of our empirical relations. At the bright end, however, the G. Popping et al. (2019) results significantly underpredict the number of galaxies with $L_{[C\,II]} > 10^9$ L$_\odot$, as their predicted LF drops well below our measurements at those luminosities.

L.-J. Liu et al. (2024) at $z = 6$ show a good agreement with our determinations, for which we show only the $\epsilon_{ff} = 0.015$ fiducial for clarity. Their model appears to be consistent with our SMF-based [C II] LF at the bright end while also showing a similarly steep faint-end slope. Their variant at $\epsilon_{ff} = 0.045$ (not shown) is also consistent across the range and within our uncertainties. However, we note that their low burstiness variant at $\epsilon_{ff} = 0.005$ predicts more [C II]-bright emitters than we infer and a shallower faint-end slope.

Both the predictions from B. Yue & A. Ferrara (2019) and M. Béthermin et al. (2022) predict the existence of extremely [C II]-bright galaxies at $z \sim 6$. B. Yue & A. Ferrara (2019) derive their $z \sim 6$ [C II] LF semi-empirically, convolving the dust-corrected $z \sim 6$ UV LF of a lognormal relation between [C II] and SFR and is thus closer in approach to our UV-LF-based method. Their bright-end excess is consistent with both our result and the M. Béthermin et al. (2022). We note, however, that this excess can also be explained by a scatter upward due to a broad $L_{[C\,II]}$–SFR relation, rather than a real population of extremely bright [C II]-emitters.

[1]*Leiden Observatory, Leiden University, PO Box 9513, NL-2300 RA Leiden, the Netherlands*
[2]*Department of Astronomy, University of Geneva, Chemin Pegasi 51, CH-1290 Versoix, Switzerland*
[3]*Cosmic Dawn Center (DAWN), Niels Bohr Institute, University of Copenhagen, Jagtvej 128, København N, DK-2200, Denmark*
[4]*Institute of Astronomy and Astrophysics, Academia Sinica, 11F of Astronomy – Mathematics Building, No. 1, Sec. 4, Roosevelt Rd, Taipei 106319, Taiwan, ROC*
[5]*Instituto de Estudios Astrofisicos, Facultad de Ingeniería y Ciencias, Universidad Diego Portales, Av. Ejército 441, Santiago, Chile*
[6]*Millennium Nucleus for Galaxies (MINGAL), Chile*
[7]*International Centre for Radio Astronomy Research (ICRAR), The University of Western Australia, M468, 35 Stirling Highway, Crawley, WA 6009, Australia*
[8]*ARC Centre of Excellence for All Sky Astrophysics in 3 Dimensions (ASTRO 3D), Australia*
[9]*Canadian Institute for Theoretical Astrophysics, 60 St George St, University of Toronto, Toronto, ON M5S 3H8, Canada*
[10]*David A. Dunlap Department of Astronomy and Astrophysics, University of Toronto, 50 St George St, Toronto, ON M5S 3H4, Canada*
[11]*Department of Physics, University of Toronto, 60 St George St, Toronto, ON M5S 3H8, Canada*
[12]*Scuola Normale Superiore, Piazza dei Cavalieri 7, I-56126 Pisa, Italy*
[13]*Jodrell Bank Centre for Astrophysics, University of Manchester, Oxford Road, Manchester M13 9PL, UK*
[14]*Center for Frontier Science, Chiba University, 1-33 Yayoi-cho, Inage-ku, Chiba 263-8522, Japan*
[15]*Hiroshima Astrophysical Science Center, Hiroshima University, 1-3-1 Kagamiyama-Higashi, Hiroshima 739-8526, Japan*
[16]*Dipartimento di Fisica 'Enrico Fermi', Università di Pisa, Largo Bruno Pontecorvo 3, I-56127 Pisa, Italy*
[17]*Astrophysics Research Institute, Liverpool John Moores University, 146 Brownlow Hill, Liverpool L3 5RF, UK*

Downloaded from academic.oup.com/mnras/article/553/2/stag2017/8994297 by Liverpool John Moores University user on 16 November 2026

[18]*Department of Astronomy, Columbia University, 550 W 120th St, New York, NY 10025, USA*
[19]*Center for Computational Astrophysics, Flatiron Institute, 162 5th Ave, New York, NY 10010, USA*
[20]*Departament d'Astronomia i Astrofisica, Universitat de València, Av. Vicent Andrés Estellés 19, E-46100 Burjassot, València, Spain*
[21]*Unidad Asociada CSIC 'Grupo de Astrofísica Extragaláctica i Cosmología' (Instituto de Física de Cantabria – Universitat de València), Spain*
[22]*Steward Observatory, University of Arizona, 933 North Cherry Avenue, Tucson, AZ 85721, USA*

This paper has been typeset from a TEX/LATEX file prepared by the author.

Downloaded from academic.oup.com/mnras/article/553/2/stag2017/8994297 by Liverpool John Moores University user on 16 November 2026

© The Author(s) 2026.
Published by Oxford University Press on behalf of Royal Astronomical Society. This is an Open Access article distributed under the terms of the Creative Commons Attribution License (https://creativecommons.org/licenses/by/4.0/), which permits unrestricted reuse, distribution, and reproduction in any medium, provided the original work is properly cited.